Annu. Rev. Fluid Mech. 2003. 35:135–67
doi: 10.1146/annurev.fluid.35.101101.161144

MIXING EFFICIENCY IN STRATIFIED SHEAR FLOWS

W. R. Peltier
Department of Physics, University of Toronto, Toronto, Ontario M5S 1A7 Canada; e-mail: peltier@atmosp.physics.utoronto.ca

C. P. Caulfield
Department of Mechanical and Aerospace Engineering, University of California, San Diego, La Jolla, California 92093-0411; e-mail: cpc@mae.ucsd.edu

Key Words stratified flows, transition

■ **Abstract** The issue of the physical mechanism(s) that control the efficiency with which the density field in stably stratified fluid is mixed by turbulent processes has remained enigmatic. Similarly enigmatic has been an explanation of the numerical value of ∼0.2, which is observed to characterize this efficiency experimentally. We review recent work on the turbulence transition in stratified parallel flows that demonstrates that this value is not only numerically predictable but also that it is expected to be a nonmonotonic function of the Richardson number that characterizes preturbulent stratification strength. This value of the mixing efficiency appears to be characteristic of the late-time behavior of the turbulent flow that develops after an initially laminar shear flow has undergone the transition to turbulence through an intermediate instability of Kelvin-Helmholtz type.

1. INTRODUCTION

In comparison with the relatively simple problem of thermal convection, the problem of understanding the mechanics of the turbulence transition in an initially laminar "free" shear layer involves a considerable increase in complexity. Whereas in the problem of thermal convection the strength of the thermal forcing is most often kept fixed by fixing the appropriate Rayleigh number and then measuring the corresponding Nusselt number (nondimensional heat transfer) in a statistical equilibrium state, in the case of the free shear layer, mixing is forced to occur through a highly time-dependent sequence of specific events that originate through a simple mechanically driven instability whose strength depends not only on the magnitude but also the structure of the vertical shear in horizontal velocity. In this problem the correct nondimensional measure of the strength of the initial mechanical forcing is the so-called gradient Richardson number Ri(z), which is defined as

$$\mathrm{Ri}(z) = \frac{\mathrm{N}^2}{(\mathrm{dV}/\mathrm{dz})^2} = \frac{(-\mathrm{gd}\ell\mathrm{og}\bar{\rho}(z)/\mathrm{dz})}{(\mathrm{dV}/\mathrm{dz})^2}, \quad (1)$$

in which $N^2(z)$ is the square of the Brunt-Vaisala frequency, $\bar{\rho}(z)$ is the height variation of the density field in the initially parallel-flow basic state, and $V(z)$ is the initial height variation of background horizontal velocity. The important theorem of Miles (1961) and Howard (1961) assures us that this stratified parallel flow will be stable against small amplitude fluctuations so long as $Ri(z) > 0.25$ at all heights. However, as soon as $Ri(z) < 0.25$ at some level in the parallel flow, a rich variety of instabilities may occur (see Drazin & Reid 1981). Although circumstances in which the stratified shear instability that arises when the Miles-Howard criterion for stability is violated may produce coherent structures other than the vortical disturbances of Kelvin and Helmholtz (KH) (see Drazin & Reid 1981), the development of these so-called KH instabilities appears to constitute the usual first step toward the onset of vigorous mixing of the density field, and they have been observed both in the atmosphere and oceans (see, e.g., Woods 1968, De Silva et al. 1996). KH instabilities are the inevitable consequence of instability in circumstances in which either the stratification is sufficiently weak or the thickness of the layer of strong, inflectional shear (see Drazin & Reid 1981) is similar to the thickness of any coincident concentration in the (stable) density gradient. Only when the latter thickness is significantly smaller than the former, and the stratification is sufficiently strong, does the characteristic instability bifurcate into the more exotic Holmboe instability (Holmboe 1962, Browand & Winant 1973, Koop & Browand 1979, Smyth et al. 1988, Lawrence et al. 1991).

The Holmboe instability is characterized at finite amplitude (see Smyth et al. 1988) by vortical disturbances displaced above and below the region of strong density gradient that propagate in opposite directions relative to the mean flow—unlike the KH instability, which is stationary in a frame of reference moving with the mean flow. The Holmboe instability also induces significant overturning of the region of strong density gradient. Experimental evidence (Browand & Winant 1973, Koop & Browand 1979, Strang & Fernando 2001) suggests that flows that exhibit Holmboe instabilities alone cause relatively weak mixing compared to the intense mixing associated with high Reynolds number and low Richardson number KH instabilities. However, some recent numerical evidence (Smyth & Winters 2002) suggests that the long time evolution of the instability (in the absence of transition) may nevertheless induce significant mixing, and experimental evidence (see Strang & Fernando 2001) suggests that the Holmboe instability may play a significant role in enhancing the mixing associated with KH breakdown at higher Richardson numbers.

Because KH instabilities may induce extremely vigorous mixing through intense three-dimensional turbulence when "transition" occurs, we focus the discussion here on explaining the mechanisms by which this can occur, concentrating on recent advances in the explanation and quantification of the time-dependent mixing behavior obtained through theoretical and numerical analyses. Because the dynamical processes that occur during the evolution of an unstable free shear layer feed back in a strongly negative fashion on the height-dependent horizontally

averaged mean state that supports the initial $Ri < 0.25$ KH instability, if the initial mean state is not continuously reinforced the process of shear-layer transition will have a finite lifetime, the end state of which will be a relaminarized mean state that is dynamically stable. This is a fundamental point that distinguishes unforced stratified shear flow evolution from forced stratified turbulence, whether the latter is realized experimentally (see Linden 1979, Fernando 1991 for reviews and, more recently, Park et al.1994, Keller & Van Atta 2000) or numerically through the maintenance of the mean shear and density profiles (Gerz et al. 1989, Holt et al. 1992, Jacobitz et al. 1997, Diamessis & Nomura 2002). As we discuss in Section 3, several important points of connection do exist between these distinct circumstances, particularly in flows with sufficiently weak stratification and large Reynolds number, as in such cases the decay of the turbulence following transition is slow enough to allow for meaningful comparison.

Analysis of the processes that occur during mixing layer development point to the utility of consideration of a discrete sequence of interactions, with the character of the flow passing through an identifiable life cycle. In order to isolate the fundamental character of these distinct stages, it is most straightforward to assume that the flow remains horizontally periodic and that the initial instability develops in time, rather than in space as it does in experiments in which the instability is forced to develop downstream from a splitter plate (see, e.g., Lawrence et al. 1991). Such analyses are therefore most directly applicable to understanding the measurements made in tilted-tube experiments such as those by Thorpe (reviewed in Thorpe 1987). Our specific goal in this review, however, is to discuss the way in which recent theoretical developments (discussed initially in the papers by Winters et al. 1995 and Winters & D'Asaro 1996, which built upon the seminal ideas of Lorenz 1955) are enabling us to make quantitative contact between numerical simulations of shear flow transition (in particular those by Caulfield & Peltier 2000 and Smyth & Moum 2000a,b) and experimental observations (Linden 1979, Fernando 1991, Strang & Fernando 2001). The accumulating data present compelling evidence that, provided the flow undergoes a true transition to turbulence, the efficiency (i.e., the ratio of irreversible increases in the potential energy of the density distribution to the irreversible loss of kinetic energy) is approximately 20%.

The identification of the sequence of secondary instabilities that control the evolution of the free shear layer, as well as that for the unstratified end member, began with the work by Peltier et al. (1978), Davis & Peltier (1979), and Klaassen & Peltier (1985b, 1989, 1991). In these papers it was first suggested on physical grounds, and then demonstrated mathematically, based on the application of rigorous Floquet methods, that once the initially two-dimensional stratified KH instability saturated, it became susceptible to a three-dimensional convective instability that was focused in the regions around the periphery of the vortex cores, or billows that characterize the "cats eye" structure of the saturated KH instability (see Figure 1, where the regions of static instability induced by the primary instability are shaded). The validity of these three-dimensional linear analyses of the stability of the two-dimensional nonlinear KH billow relied on the assumption of a

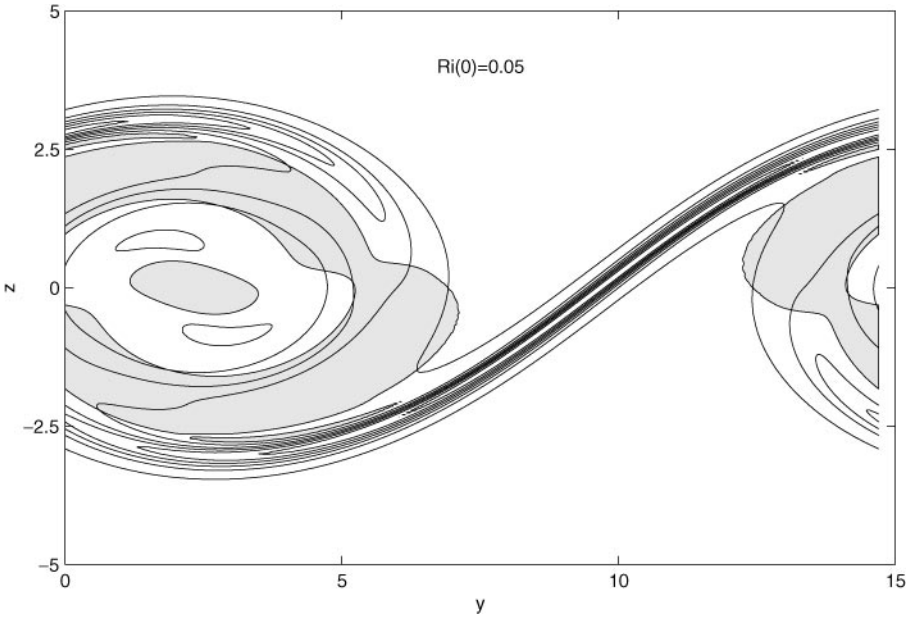

Figure 1 Contours of spanwise vorticity at a time when the primary KH billow has maximum amplitude in a stratified shear flow with initial hyperbolic tangent velocity and density profiles. Re $= 750$, Pr $= 1$, and minimum gradient Richardson number Ri(0) $= 0.05$. Statically unstable regions are shaded. [Adapted from Figure 1*b* in Caulfield & Peltier (2000), used with permission.]

separation of timescales between the two-dimensional KH billow and the incipient three-dimensional instability, an assumption that was verified a posteriori.

Three-dimensional direct numerical simulations were required to test the validity of these theoretical predictions, and the analyses described by Caulfield & Peltier (1994) fully confirmed the prediction that the secondary instability should consist of a shear aligned convective disturbance focused in regions of overturned isopycnals caused by the "rolling-up" of the vorticity in the original shear layer. The more detailed analyses by Caulfield & Peltier (2000) further demonstrated the validity of the theoretical prediction that this secondary mode of transition for stratified flow was fundamentally different from that which controls the transition to turbulence in the unstratified case. Although the appearance of streamwise oriented streaks of vorticity are observed to be precursory to turbulent collapse in both cases, in the unstratified case these streaks originate in a hyperbolic instability that is focused on the hyperbolic stagnation points that exist between successive billow cores, as first suggested on theoretical grounds by Klaassen & Peltier (1991). This result contradicted the earlier suggestion that it was the elliptical instability, localized on the elliptical stagnation point interior to the primary KH billow, as had been earlier suggested by Pierrehumbert & Widnall (1982), that was responsible

for transition in the unstratified case (see Kerswell 2002 for a thorough review of the elliptical instability).

As we review in detail here, the efficiency of the mixing that occurs immediately after the initially two-dimensional nonlinear KH instability matures is rather high, typically of the order of 70%. Crucially, this mixing is associated with convective overturning of the statically unstable regions in the periphery of the primary billow, which trigger the onset of the three-dimensional convective instability, and is "efficient" because the flow is in no way turbulent at this stage. Therefore, the viscous dissipation is relatively close to its laminar value, and thus a significant proportion of the energy being lost irreversibly from the velocity shear is leading to irreversible increases in flow potential energy. The relative importance of this stage is, unsurprisingly, strongly dependent on the flow Reynolds number and overall stratification, as we show below, and for sufficiently small Richardson numbers, and sufficiently large Reynolds numbers, the mixing associated with this stage can be completely overwhelmed by turbulent mixing associated with the breakdown of the finite amplitude saturated structures owing to the convective instability.

This point, that the dominant mixing processes for a stratified shear flow are driven by secondary convective instabilities that are catalyzed by the primary instability and thus act as the most significant "injection scale" for the ensuing turbulent cascade and irreversible mixing, lies at the heart of the discussion to follow. To make this clear, it is necessary to quantify the relative importance of mixing events within the dynamically evolving flow as well as the evolution of flow energetics, in particular, the exchanges between the kinetic energy and potential energy reservoirs. In Section 2, we therefore discuss a framework that may be employed to achieve this, essentially by compartmentalization of the potential energy of the flow into two parts, the background or minimum potential energy and the available potential energy, as suggested by Winters and coworkers (Winters et al. 1995, Winters & D'Asaro 1996), whose methodology builds on the ideas of Lorenz (1955). Furthermore, this framework is a generalization to three dimensions of a methodology suggested earlier by Thorpe (1977). It is important to note that a somewhat similar approach was proposed independently by Scinocca (1995).

Use of this compartmentalization, and appropriately defined mixing efficiencies that may be derived from it, has recently led to a clear understanding as to why experimental measures of mixing efficiency have invariably led to estimates on the order of 0.2. In Section 3 we summarize the results of numerical simulations of transitional shear flows, results that point toward the crucial importance of late-time turbulence transition to understanding the mixing properties of stratified flows at sufficiently high Reynolds number and sufficiently low characteristic Richardson number. In Section 4 we focus our attention on this late stage of flow evolution in which transition occurs, demonstrating that mixing efficiency is expected to be a nonmonotonic function of the Richardson number, a result that has extremely important and well-known dynamical consequences involving the

tendency of a turbulent flow of density-stratified fluid to induce a step-discontinuous "staircase" structure in the height variation of horizontally averaged density, as originally proposed by Phillips (1972) and Posmentier (1977) and subsequently discussed by various authors (Linden 1979, Barenblatt et al. 1993, Balmforth et al. 1998). We discuss the implications of our results in comparison with these recent theoretical investigations as well as experiments (in particular those by Strang & Fernando 2001), concentrating on the issues of mixing efficiency and hence layer formation. In Section 5 we offer conclusions and a discussion of outstanding questions.

2. BACKGROUND AND AVAILABLE POTENTIAL ENERGY IN STRATIFIED FLUIDS

The utility of the compartmentalization of the potential energy of a flow into two parts can best be appreciated by consideration of the evolution equations for the total flow kinetic energy and potential energy. For simplicity, we concentrate on the simple circumstance (typically characteristic of numerical simulations) in which the horizontal boundaries are periodic so that there is no net transport into or out of the domain. We also assume that the upper and lower boundaries are insulating so that there is no flux of density into or out of the domain (see Winters et al. 1995 for a discussion of the boundary contributions in more general circumstances). Because we are interested in stratified shear flows, we assume (as is conventional) that there is some characteristic total velocity difference $2V_0$, with characteristic shear-layer depth $2d_0$, and total density difference $2\rho_0$. We further assume that the fluid is Boussinesq so that the variations in density are sufficiently small compared to some characteristic reference density and that they are only significant in the buoyancy force. Therefore, using ρ_0, d_0, and the advective time scale d_0/V_0, the nondimensional governing equations (for a fluid with kinematic viscosity ν and density diffusivity κ) are

$$\frac{Du_i}{Dt} = -\frac{\partial p'}{\partial x_i} - Ri_o\, \rho'\, \delta_{i3} + \frac{1}{Re}\frac{\partial^2 u_i}{\partial x_j^2}, \tag{2a}$$

$$\frac{\partial u_i}{\partial x_i} = 0, \tag{2b}$$

$$\frac{D\rho'}{Dt} = \frac{1}{Re\, Pr}\frac{\partial^2 \rho'}{\partial x_j^2}, \tag{2c}$$

where ρ' and p' are the perturbation density and pressure, respectively, Pr is the Prandtl number ν/κ, $Re = V_0 d_0/\nu$ is the Reynolds number, and Ri_0 is the bulk Richardson number $g\, \rho o\, d_0/V_0^2$, an overall measure of the relative importance of the stratification compared to the inertia of the flow. With the appropriate boundary conditions described above, the evolution of the kinetic energy $\mathcal{K}$ per unit volume

of the flow governed by Equations 2a–c satisfies the equation

$$\frac{d\mathcal{K}}{dt} = -Ri_o\langle\langle\langle\rho w\rangle_x\rangle_y\rangle_z - \frac{1}{Re}\langle\langle\langle(\underline{\nabla}u)^2\rangle_x\rangle_y\rangle_z \tag{3a}$$

$$= \mathcal{H} - \varepsilon, \tag{3b}$$

with

$$\mathcal{K} = \langle\langle\langle(u^2 + v^2 + w^2)/2\rangle_x\rangle_y\rangle_z, \tag{3c}$$

where angle brackets denote averaging over the subscripted coordinate direction. Similarly the potential energy $\mathcal{P}$ of the flow governed by Equations 2a–c satisfies the evolution equation

$$\frac{d\mathcal{P}}{dt} = -\mathcal{H} + \mathcal{D}_p, \tag{4a}$$

with

$$\mathcal{P} = Ri_o\langle\langle\langle\rho z\rangle_x\rangle_y\rangle_z \tag{4b}$$

and

$$\mathcal{D}_p = \frac{Ri_o(\overline{\rho}\,\langle\text{bottom, t}\rangle - \overline{\rho}\,(\text{top, t}))}{Z\,Re\,Pr}, \tag{4c}$$

where Z is the nondimensional height of the domain, and $\overline{\rho}$ (bottom) and $\overline{\rho}$ (top) are the nondimensional densities at the bottom and top boundaries, respectively.

$\mathcal{D}_p$ is the rate at which the potential energy of a statically stable density distribution would increase in the absence of macroscopic fluid motion (essentially through conversion of internal energy into potential energy), and so for sufficiently deep flow domains this plays no significant dynamical role in flow evolution. We wish to distinguish this increase from "mixing" because we prefer to consider mixing as involving irreversible changes in fluid properties that are directly associated with macroscopic fluid motions, rather than those changes that would occur in a diffusive, macroscopically quiescent, system.

The crucial term for the quantification of mixing in these equations is, of course, the heat flux, or buoyancy flux $\mathcal{H}$, which quantifies the exchange between the kinetic and potential energy reservoirs. However, fluid motions can increase the potential energy of the system by two qualitatively different processes, namely, by either "mixing" or "stirring." Any lifting (on average) of anomalously dense fluid by the flow (hence involving negative values of $\mathcal{H}$) will lead to an increase of potential energy. However, this increase is only irreversible (and so is appropriately identified with mixing) if diffusion acts on sufficiently small scales so as to change the density of the lifted fluid parcel, as well as its neighbors. Such mixing is inevitably irreversible and acts over the small length scales characteristic of diffusion. Otherwise, the lifted parcels may later fall under gravity, reconverting the

temporarily stored potential energy into kinetic energy, a process that is identified as stirring (a larger-scale process that is nondiffusive).

It should be clear, therefore, that instantaneous values of the buoyancy flux $\mathcal{H}$ can be very misleading as a proxy for mixing, particularly in flows with significant time variability. Irreversible increases in potential energy owing to fluid motion can only be distinguished from the buoyancy flux through averaging over sufficiently long timescales so that the reversible effects of stirring completely cancel out. Clearly, such averaging is not always possible in the laboratory or in the analysis of oceanographic or meteorological data. However, the formalism of Winters et al. (1995) does enable the time-dependent separation of mixing from stirring processes because variations in the background potential energy can be identified directly with mixing and the diffusion of the mean profile quantified by $\mathcal{D}_{\mathrm{p}}$ (which these authors have referred to as Φ_{i}).

We define the dimensional background potential energy $\mathcal{P}_{\mathrm{B}}$(t) as

$$\mathcal{P}_B\,(t) = \langle \mathrm{g}\rho_{\mathrm{B}}\,(\mathrm{z},\,t)\,\mathrm{z}\rangle_{\mathrm{z}}. \tag{5}$$

In Equation 5, ρ_{B}(z, t) is the notional one-dimensional density distribution generated (by volume conserving adiabatic rearrangement of fluid elements) from the actual density distribution ρ(x, y, z, t) at the time t that is everywhere statically stable. In general, the background potential energy is the minimum potential energy that the flow can have, and this energy cannot be extracted from the potential energy reservoir to drive (macroscopic) fluid motions, i.e., energy stored in $\mathcal{P}_{\mathrm{B}}$ is inaccessible to stirring. Following Lorenz (1955), we then define an available potential energy $\mathcal{P}_{\mathrm{A}}$ that is, at least in principle, available to the kinetic energy reservoir for stirring as

$$\mathcal{P}_{\mathrm{A}} = \mathcal{P} - \mathcal{P}_{\mathrm{B}}, \tag{6}$$

where $\mathcal{P}$ is the instantaneous total potential energy of the flow as defined in Equation 4b.

$\mathcal{P}_{\mathrm{A}} > 0$ if there exists any lateral variations in density or statically unstable regions. In Figure 2, we provide a schematic illustration of just such an adiabatic rearrangement of fluid elements, showing that the generation of ρ_{B} can involve changes in shape, but not the volume of the individual elements, and that the total potential energy (defined by the mean density profile) is always bounded below by the background potential energy.

In the absence of macroscopic fluid motion, $\mathcal{P}_{\mathrm{B}}$ will increase through the effect of $\mathcal{D}_{\mathrm{p}}$, as defined in Equation 4c, as the mean profile diffuses. Crucially, $\mathcal{P}_{\mathrm{B}}$ can also increase through irreversible mixing processes, and thus it is possible to partition the buoyancy flux into two distinct terms and to write distinct evolution equations for $\mathcal{P}_{\mathrm{A}}$ and $\mathcal{P}_{\mathrm{B}}$ as

$$\frac{\mathrm{d}\mathcal{P}_{\mathrm{A}}}{\mathrm{dt}} = -\mathcal{H} - \mathcal{M}, \tag{7a}$$

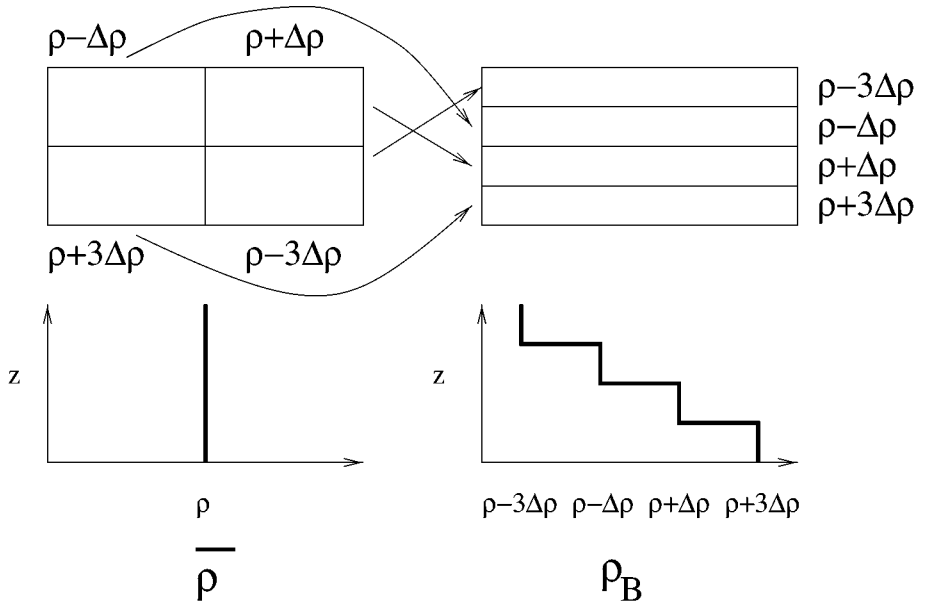

Figure 2 Schematic diagram of the adiabatic redistribution of fluid parcels (with densities in the range $\rho +/- 3\Delta\rho$) to evaluate the background density distribution ρ_B associated with the minimal background potential energy $\mathcal{P}_B$ of a flow. Note that the fluid parcels change shape but not volume. Also shown are the vertical distributions of the mean density ρ and the background density distribution ρ_B. [Adapted from figure 3 in Caulfield & Peltier (2000), used with permission.]

$$\frac{d\mathcal{P}_B}{dt} = \mathcal{M} + \mathcal{D}_P, \tag{7b}$$

thereby defining an irreversible mixing rate $\mathcal{M}$. The stirring rate is then $\mathcal{S} = -\mathcal{H} - \mathcal{M}$. Over sufficiently long time integrations, the integral of the stirring rate is zero. Winters et al. (1995) referred to the sum of the terms on the right-hand side of Equation 7b as Φ_B. In our view, it is most appropriate to consider the mixing rate $\mathcal{M}$ and the term $\mathcal{D}_p$ to be distinct, as this subdivision isolates the component of the increase in $\mathcal{P}_B$ that originally came from the kinetic energy reservoir and thus is inherently related to macroscopic fluid motions. When there is fluid motion, kinetic energy enters the potential energy reservoir through the buoyancy flux $\mathcal{H}$, leading to increases (at least briefly) in the available potential energy $\mathcal{P}_A$. Mixing (increases in $\mathcal{P}_B$) is associated with an imperfect return of this potential energy to the kinetic energy reservoir, so for mixing to occur it is necessary that there be some available potential energy in the system.

For fluid motions to enhance diffusive transport, and hence the rate of increase of $\mathcal{P}_B$, two distinct phenomena must be involved. First, local gradients of density

must be intensified to enhance the flux. However, this is only half the story: In order to enhance transport, the area over which the flux enhancement occurs must also increase, implying the need for neighboring density isosurfaces to become complicated through the development of small scales of motion. A dense parcel, feeling a buoyancy force restoring it to its neutral buoyancy height, will tend to cause both these effects: Local gradients in density will intensify owing to the parcel's motion (thus enhancing diffusive flux), and also, critically, the conversion of potential to kinetic energy will tend to introduce small scales, thus enhancing transport. As we discuss below, such behavior can be directly identified and understood in transitional shear flows but can also be found in forced stratified turbulence, provided that the flow exhibits regions of overturning (e.g., see Diamessis & Nomura 2002).

Indeed, a particular attraction of this formalism is that it is exceedingly straightforward to implement in a numerical simulation, as suggested by Winters et al. (1995). At any particular time step, sorting algorithms can be used to order by their density the *n* individual fluid elements located in the *n* grid volume elements in the computational domain. These fluid parcels can then be notionally placed into a purely one-dimensional array, created by deforming the *n* grid volume elements (while conserving volume) into *n* thin horizontal layers extending across the whole flow domain. [See Caulfield & Peltier (2000) for a more detailed discussion, generalizing Winters et al. (1995), who proposed using the nondeformed grid, thus allowing for horizontal density variations and hence generating only an approximate upper bound to ρ_{B}.] This notional deformed grid, corresponding to the identification of a unique height with each of the fluid elements arrayed within a monotonic density field, creates the background density profile $\rho_{\mathrm{B}}(z)$ and hence $\mathcal{P}_{\mathrm{B}}$. As originally pointed out by Winters et al. (1995), and discussed further by Tseng & Ferziger (2001), such sorting and reordering is intimately related to construction of the probability density function for the fluid density. Numerically, this procedure can be performed at every time step, and so the time evolution of $\mathcal{P}_{\mathrm{B}}$ can be followed, thus identifying the time dependence of the irreversible mixing that is occurring.

It is of course important to quantify not only the absolute amount of mixing that occurs, but also its efficiency, i.e., the proportion of the kinetic energy lost by the fluid that leads to mixing, as opposed to that which is lost to viscous dissipation. In the discussion to follow, we make use of a definition of instantaneous mixing efficiency, say, $\mathcal{E}_{\mathrm{i}}$, that we define as

$$\mathcal{E}_i = \frac{\mathcal{M}}{\mathcal{M} + \varepsilon}. \tag{8a}$$

Because the viscous dissipation ε is positive-definite, it is clear that $\mathcal{E}_{\mathrm{i}} \leq 1$, as is required on physical grounds. The denominator here represents the irreversible losses of kinetic energy owing to both irreversible mixing and viscous dissipation.

We may also define a cumulative mixing efficiency in the obvious way as

$$\mathcal{E}_c = \frac{\int_0^t \mathcal{M}(u)\,du}{\int_0^t \mathcal{M}(u)\,du + \int_0^t \varepsilon(u)\,du}, \tag{8b}$$

where the time interval may be selected so as to isolate the manner in which mixing efficiency changes over a series of appropriately selected epochs during flow evolution. Such a definition eliminates the diffusive contribution $\mathcal{D}_P$, as this is not associated with the kinetic energy, and hence the macroscopic fluid motion of the system.

This elimination allows an identification of the cumulative mixing efficiency, integrated over a sufficiently long time, with the flux Richardson number as was defined by Linden (1979), namely, as "the fraction of the change of the available kinetic energy which appears as the potential energy of the stratification." This is appropriate because it allows for the long-term cancellation of the influence of those large-scale processes that we refer to as stirring. However, the flux Richardson number R_f is often defined as

$$R_f = \frac{-\mathcal{H}}{-\mathcal{H} + \varepsilon}. \tag{9a}$$

or, indeed, in sheared flows as

$$R_f = \frac{-\mathcal{H}}{\overline{u'w'}\,dV/dz}. \tag{9b}$$

(see, e.g., Strang & Fernando 2001), these two definitions being equivalent if the system is closed, i.e., the turbulent kinetic energy is statistically steady and dominates the dissipation occurring within the flow.

The flux Richardson number is a parameter that lies at the heart of the parameterizations of mixing within turbulent closure schemes (see, e.g., Mellor & Yamada 1982). Here, we are interested in the mechanisms responsible for causing, and the quantification of, stratified mixing within transitional stratified shear flows, and in such fundamentally time-dependent circumstances, R_f would be an adequate definition of mixing efficiency if the entire increase of potential energy caused by the vertical flux of buoyancy $-\mathcal{H}$ were irreversibly converted into an increase of background potential energy $\mathcal{P}_B$. However, it is inevitable that some (often very significant) fraction of $\mathcal{H}$ is simply associated with reversible stirring, and so it should be clear that our definitions of mixing efficiency are most appropriate when the required data are available, as is the case in numerical simulations.

Our procedure for the determination of mixing efficiency in stably stratified parallel flows reviewed above is essentially a three-dimensional generalization of the one-dimensional reordering proposed by Thorpe (1977) to assess the size of overturning regions from one-dimensional observational profiles, generating the so-called Thorpe scale L_T. His scale is based on the reordering of individual density measurements in such a way as to generate a stable vertical profile. Such sorting enables one to generate an array of "Thorpe displacements" δ_j for each of the

density parcels. From these, one defines the Thorpe scale $L_T = (\overline{\delta_j^2})^{1/2}$ as the rms of the displacements. Flows in which mixing is intense are then flows in which the Thorpe scale is large. Smyth & Moum (2000b) have examined in detail the connection between the Thorpe scale and the characteristic scales of reordering within a three-dimensional framework.

As described below, construction of the subdivision of the potential energy into $\mathcal{P}_B$ and $\mathcal{P}_A$, together with a consideration of the time-dependent evolution of these fields, the quantities $\mathcal{M}$ and $\mathcal{S} = -\mathcal{H} - \mathcal{M}$, and the mixing efficiencies defined in Equation 8, yield valuable insight into the nature of the mixing that occurs in stratified shear flows.

3. THE ANATOMY OF THE MIXING TRANSITION IN STRATIFIED PARALLEL FLOW

In reviewing recent work on the detailed sequence of dynamical events that occurs during the process of transition from a laminar state of stratified parallel flow to a state of intense three-dimensional turbulence, it is useful to discuss the various regimes of flow sequentially. There are essentially three distinct phases in the evolution of such flows: (*a*) the stage of initial parallel shear instability and subsequent KH wave growth to saturation amplitude, (*b*) the stage of onset and growth of the three-dimensional secondary instability through which shear aligned convective rolls are nucleated in the region surrounding the KH billow cores, and finally, (*c*) the stage of turbulent-mixing layer collapse characterized by intense viscous dissipation and triggered fundamentally by the breakdown of the shear aligned convective rolls that grow on, and then destroy, the primary KH billow. These three stages of the mixing transition are illustrated qualitatively in Figure 3, where we show isosurfaces of cross-stream and streamwise vorticity from a direct numerical simulation (DNS) in which the streamwise length of the domain is restricted to a single wavelength of the fastest growing mode of the linear instability through which the transition process is initially engendered. Below, we discuss these stages in the mixing process in sequence.

3.1. The Kelvin-Helmholtz Stage of Flow Evolution

To illustrate through specific examples the sequence of events that occurs during the transition to turbulence in the stratified shear layer, we consider an initial state characterized by background profiles of horizontal streamwise velocity $\bar{V}(z)$ and density $\bar{\rho}(z)$ in the form

$$\bar{V}(z) = V_o \tanh(z/d), \tag{10a}$$

$$\bar{\rho}(z) = \rho_a + \rho_o \tanh(Rz/d), \tag{10b}$$

in which $R = 1.1$ is the ratio of the thickness of the shear layer to the thickness of the density inversion and is chosen to enable close accord with conditions achievable in laboratory experiments (e.g., Thorpe 1987) and to be susceptible to instabilities of KH type. This flow has been considered by many authors (Caulfield & Peltier 1994, 2000; Palmer et al. 1994, 1996; Cortesi et al. 1998; Smyth & Moum 2000a,b). We briefly review what we perceive to be the key characteristics of the transition to a stage of intense turbulent mixing in these flows, focusing on the critical importance of the secondary convective instability to flow evolution as well as the variation of the mixing characteristics with stratification. For these profiles, the initial gradient Richardson number is minimum at the midpoint of the shear layer and equals $Ri(0) = R\,Ri_0$, where Ri_0 is the bulk Richardson number of the initially parallel flow. We discuss eight different simulations in detail here, all with $Pr = 1$; $Re = 750$; and $Ri(0) = 0$, 0.025, 0.05, 0.0625, 0.075, 0.0875, 0.1, and 0.125. This Reynolds number is comparable with that usually realized in laboratory experiments. Such a detailed investigation of the isolated effect of the variation in stratification enables us to identify clearly the nature of the nonmonotonicity of the variation of the mixing efficiency with stratification, although it is important to stress that it is also of great interest to understand the effect of varying the other characteristic flow parameters (see Klaassen & Peltier 1985a; Smyth & Moum 2000a,b; Smyth et al. 2001 for a discussion of the effect of variation in Pr). We return to this point in Section 5.

We have also chosen the density stratification to vanish in the region exterior to the region of strong shear. When the exterior region is also stably stratified, internal waves may be emitted from the region of turbulent collapse and the nature of the evolution of the turbulent flow may be significantly affected. This interesting source of complexity is not addressed here (see Sutherland & Peltier 1994, 1995; Sutherland et al. 1994; Werne & Fritts 1999 for consideration of the behavior of flows in which the influence of external stratification is included).

For all the flows that we consider, the primary KH instability develops in a completely two-dimensional manner, with an initial exponential growth rate that is well predicted by linear theory and that eventually saturates at nondimensional time $t \approx 40$–60, with this saturation time being dependent on initial stratification. As discussed in detail by Caulfield & Peltier (2000), the roll-up of the primary billow leads to significant increases in the available potential energy $\mathcal{P}_A$, which is associated with the development of the statically unstable regions at the periphery of the primary billow (as is apparent in Figure 1). There also is typically little irreversible mixing before the primary billow saturates. At this saturation time, the primary billows are usually very coherent, although the outer-scale Reynolds number (defined by the vertical extent of the billow and the total velocity jump) is on the order of 10^4 and so is sufficiently high for us to expect a turbulence transition (see Dimotakis 2000 for further discussion). This is naturally due to the evolution of the flow in two dimensions: As the flow becomes three dimensional, its character changes qualitatively (see below).

3.2. The Stage in Which Secondary Instability of the Kelvin-Helmholtz Structure Occurs

Indeed, as the two-dimensional KH billows saturate, they become susceptible to disruption by a family of three-dimensional secondary instabilities that begin to grow precisely at the instant when the KH billow reaches its maximum amplitude. The stratified KH billow is not a stable flow configuration, owing critically to the significant value of the available potential energy $\mathcal{P}_A$, which is associated with the convectively unstable regions at the periphery of the primary billow cores. The properties of these secondary instabilities may be accurately deduced on the basis of a detailed Floquet analysis. Subject to the assumption that the three-dimensional perturbations to the two-dimensional nonlinear KH billow remain small, we represent them in the form

$$\underline{u}_{3D}(x, y, z, t) = \hat{u}_{3D}(y, z, t) \exp[i\gamma x + i\delta y], \tag{11a}$$

$$\rho_{3D}(x, y, z, t) = \hat{\rho}_{3D}(y, z, t) \exp[i\gamma x + i\delta y], \tag{11b}$$

where x is the spanwise direction and y is the streamwise direction. Restricting attention to fluctuations of streamwise (y) wavenumber equal to or greater than the wavenumber α_{KH} of the two-dimensional KH instability, we set the Floquet exponent δ to zero. The spectrum of subharmonic merging instabilities has been discussed in detail by Klaassen & Peltier (1989). As shown in the simulations by Cortesi et al. (1998) and Smyth & Moum (2000b), the transition to turbulence within a stratified shear flow is an inherently three-dimensional process, with two-dimensional merging events still yielding a highly coherent state, that is destroyed by the development of three-dimensional structures that such detailed stability analyses can identify.

Subject to the assumption that the three-dimensional secondary instabilities grow so rapidly that the two-dimensional KH billow may be assumed to be time independent, the dependence of $\hat{u}_{3D}$ and $\hat{\rho}_{3D}$ on space and time becomes separable. We may therefore assume

$$\hat{u}_{3D}(y, z, t) = u^{\dagger}_{3D}(y, z)e^{\sigma t}, \tag{12a}$$

$$\hat{\rho}_{3D}(y, z, t) = \rho^{\dagger}_{3D}(y, z)e^{\sigma t}, \tag{12b}$$

with, in general, the complex growth rate of $\sigma = \sigma_r + i\sigma_i$. The linear partial differential equations satisfied by the fields $\underline{u}^{\dagger}_{3D} = (u^{\dagger}_{3D}, v^{\dagger}_{3D}, w^{\dagger}_{3D})$, $\rho^{\dagger}_{3D}$ and the perturbation pressure $p^{\dagger}_{3D}$, in which $\underline{u}_{2D} = (0, v_{2D}, w_{2D})$ and ρ_{2D} are the velocity and density fields of the two-dimensional Kelvin-Helmholtz wave, are as follows:

$$\sigma u^{\dagger}_{3D} + v_{2D}\frac{\partial u^{\dagger}_{3D}}{\partial y} + w_{2D}\frac{\partial u^{\dagger}_{3D}}{\partial z} = -i\gamma\, p^{\dagger}_{3D} + \frac{1}{Re}D_2\, u^{\dagger}_{3D} \tag{13a}$$

$$\sigma v_{3D}^{\dagger} + v_{2D}\frac{\partial v_{3D}^{\dagger}}{\partial y} + w_{2D}\frac{\partial v_{3D}^{\dagger}}{\partial z} + v_{3D}^{\dagger}\frac{\partial v_{2D}}{\partial y} + w_{3D}^{\dagger}\frac{\partial v_{2D}}{\partial z} = -\frac{\partial p_{3D}^{\dagger}}{\partial y} + \frac{1}{Re}D_2 v_{3D}^{\dagger} \tag{13b}$$

$$\sigma w_{3D}^{\dagger} + v_{2D}\frac{\partial w_{3D}^{\dagger}}{\partial y} + w_{2D}\frac{\partial w_{3D}^{\dagger}}{\partial z} + v_{3D}^{\dagger}\frac{\partial w_{2D}}{\partial y} + w_{3D}^{\dagger}\frac{\partial w_{2D}}{\partial z} =$$

$$-\frac{\partial p_{3D}^{\dagger}}{\partial z} - R_{io}\rho_{3D}^{\dagger} + \frac{1}{Re}D_2 w_{3D}^{\dagger} \tag{13c}$$

$$\sigma \rho_{3D}^{\dagger} + v_{2D}\frac{\partial \rho_{3D}^{\dagger}}{\partial y} + w_{2D}\frac{\partial \rho_{3D}^{\dagger}}{\partial z} + v_{3D}^{\dagger}\frac{\partial \rho_{2D}}{\partial y} + w_{3D}^{\dagger}\frac{\partial \rho_{2D}}{\partial z} = \frac{1}{RePr}D_2 \rho_{3D}^{\dagger} \tag{13d}$$

$$\mathrm{i}\gamma \mathrm{u}_{3D}^{\dagger} + \frac{\partial \mathrm{v}_{3D}^{\dagger}}{\partial y} + \frac{\partial \mathrm{w}_{3D}^{\dagger}}{\partial z} = 0, \tag{13e}$$

where the operator $D_2 = -\gamma^2 + \partial^2/\partial y^2 + \partial^2/\partial z^2$. Because the pressure perturbation may be determined on the basis of the following diagnostic equation,

$$D_2\, p_{3D}^{\dagger} = -2\left[\left(\frac{\partial v_{2D}}{\partial y}\right)\left(\frac{\partial v_{3D}^{\dagger}}{\partial y}\right) + \left(\frac{\partial w_{2D}}{\partial z}\right)\left(\frac{\partial w_{3D}^{\dagger}}{\partial z}\right) + \left(\frac{\partial v_{2D}}{\partial z}\right)\left(\frac{\partial w_{3D}^{\dagger}}{\partial y}\right) + \left(\frac{\partial w_{2D}}{\partial y}\right)\left(\frac{\partial v_{3D}^{\dagger}}{\partial z}\right)\right] - \mathrm{Ri}_o\frac{\partial \rho_{3D}^{\dagger}}{\partial y}, \tag{13f}$$

we may eliminate $p_{3D}^{\dagger}$ from the set (Equation 13). Thus, $u_{3D}^{\dagger}$ is also removed, thereby reducing the eigenvalue problem for σ to one involving only $v_{3D}^{\dagger}$, $w_{3D}^{\dagger}$, and $\rho_{3D}^{\dagger}$. This system may be solved using a Galerkin method, which has the advantage of rapid convergence.

To implement the Galerkin methodology, we expand the unknown fields on a basis of orthogonal functions chosen such that the boundary conditions are satisfied automatically. Specifically, we take

$$\left(v_{3D}^{\dagger}, w_{3D}^{\dagger}, \rho_{3D}^{\dagger}\right) =$$

$$\sum_{m=-\infty}^{+\infty}\sum_{n=o}^{\infty}(A_{mn}\cos[n\pi(z-H)/H], B_{mn}\sin[\ ], C_{mn}\cos[\ ])e^{im\alpha_{KH}y}. \tag{14}$$

Substitution of these expansions into Equations 13a–e, followed by computation of the inner product of each of the equations in the set by each of the members of the Galerkin basis in turn, delivers the following set of algebraic equations for the Galerkin amplitudes A_{mn}, B_{mn}, and C_{mn}:

$$\sigma A_{pq} = \langle AA \rangle_{pq}^{mn} A_{mn} + \langle AB \rangle_{pq}^{mn} B_{mn} + \langle AC \rangle_{pq}^{mn} C_{mn}, \tag{15a}$$

$$\sigma B_{pq} = \langle BA \rangle_{pq}^{mn} A_{mn} + \langle BB \rangle_{pq}^{mn} B_{mn} + \langle BC \rangle_{pq}^{mn} C_{mn}, \tag{15b}$$

and

$$\sigma C_{pq} = \langle CA \rangle_{pq}^{mn} A_{mn} + \langle CB \rangle_{pq}^{mn} B_{mn} + \langle CC \rangle_{pq}^{mn} C_{mn}. \tag{15c}$$

Expressions for the four-dimensional coefficient arrays $\langle AA \rangle$, $\langle AB \rangle$, etc., are provided by Smyth & Peltier (1994). By imposing a particular truncation scheme upon the Galerkin expansions (Equation 14), specifically we use $2|m| + n \leq N$, and by taking $N = 41$ so that adequate resolution is achieved, Equation 15 then poses a standard matrix eigenvalue problem for the eigenvalue σ. A single eigenvector is defined simply by concatenating the unknowns A_{pq}, B_{pq}, and C_{pq} into a single vector V with a single running subscript. Potylitsin & Peltier (1998, 1999) have illustrated the eigenfunctions obtained in such analyses, including the impact of background rotation parallel to the axis of the KH vortex tubes, by directly contouring the three-dimensional perturbation vorticity field.

In Figure 4, we plot the real part of the eigenvalue σ, the growth rate σ_r, as a function of the spanwise wavenumber γ of the fastest growing three-dimensional perturbation for $Ri(0) = 0$, 0.025, 0.05, and 0.1. On each diagram, the globally most unstable mode is shown as the open circle. In the unstratified case, the growth rate for the subdominant elliptical core mode is also indicated. Figure 5 shows the cross-stream average over a wavelength $2\pi/\gamma$ of the perturbation kinetic energy $\mathcal{K}_{3D}$ determined on the basis of the eigenfunction of the most unstable mode from

$$\mathcal{K}_{3D} = \frac{1}{2}\left\langle \left(|u_{3D}^{\dagger}|^2 + |v_{3D}^{\dagger}|^2 + |w_{3D}^{\dagger}|^2 \right) \right\rangle_x. \tag{16}$$

Inspection of these results demonstrates that the fastest growing mode of three-dimensional secondary instability becomes more sharply confined to the statically unstable periphery of the individual billow cores as the strength of the ambient stratification increases. Only in the limit where the background stratification vanishes entirely does the mode become focused on the hyperbolic stagnation points that are located between adjacent billow cores. In Figure 5*a*, we show not only $\mathcal{K}_{3D}$ for the hyperbolic mode, but also $\mathcal{K}_{3D}$ for the elliptical core mode by Pierrehumbert & Widnall (1982), the latter denoted by the heavy solid contours in the billow core of the unstratified flow.

That these predictions of the linear stability analysis of finite amplitude KH billows are precisely borne out by complete DNS solutions of the initial value problem is demonstrated in Figure 6, where isosurfaces of spanwise vorticity and streamwise vorticity from two typical three-dimensional DNS integrations over the range of time during which the streamwise vortex streaks have just emerged from the background two-dimensional KH flow of finite amplitude are shown. Results for both the unstratified flow and the stratified flow for which

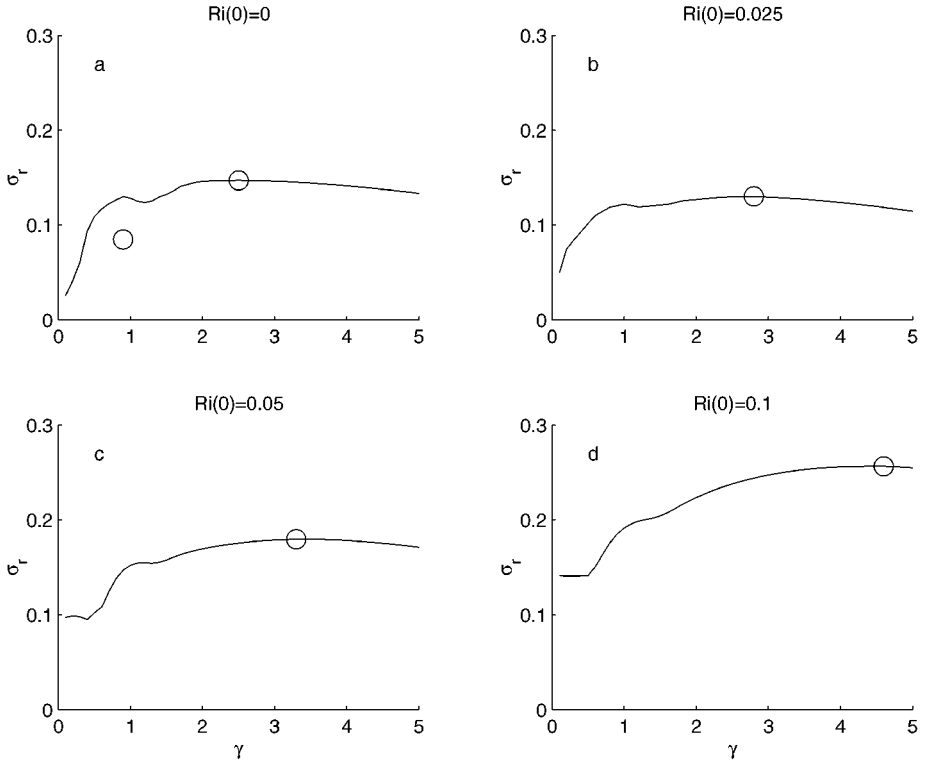

Figure 4 Predicted growth rate σ_r of the most unstable three-dimensional mode against spanwise wavenumber γ for Ri(0) = (*a*) 0, (*b*) 0.025, (*c*) 0.05, and (*d*) 0.1. In each case, the globally most unstable mode (and for the unstratified flow, the most unstable core-centered mode) is marked with a circle.

the strength of the stratification is characterized by Ri(0) = 0.05 are also shown. Intercomparison of the results for the unstratified flow (*top*) and the stratified flow (*bottom*) demonstrates that the distinctly different regions of localization of the secondary instability that is predicted by the Floquet analysis is precisely borne out by the DNS results. In the unstratified case, streamwise vortex streaks originate through instability focused on the hyperbolic stagnation points that separate adjacent billow cores, whereas in stratified flow, these streaks originate through convective instability in the regions of overturned isopycnals. Their development is triggered by a single convective overturning (releasing available potential energy to the kinetic energy reservoir) in the statically unstable regions at the periphery of the primary cores. Their growth is also driven by the background shear, with the relative importance of these two processes depending on the overall stratification (see Caulfield & Peltier 2000 for further discussion). Furthermore, the critical importance of these streamwise vortices for the transition to turbulence is confirmed

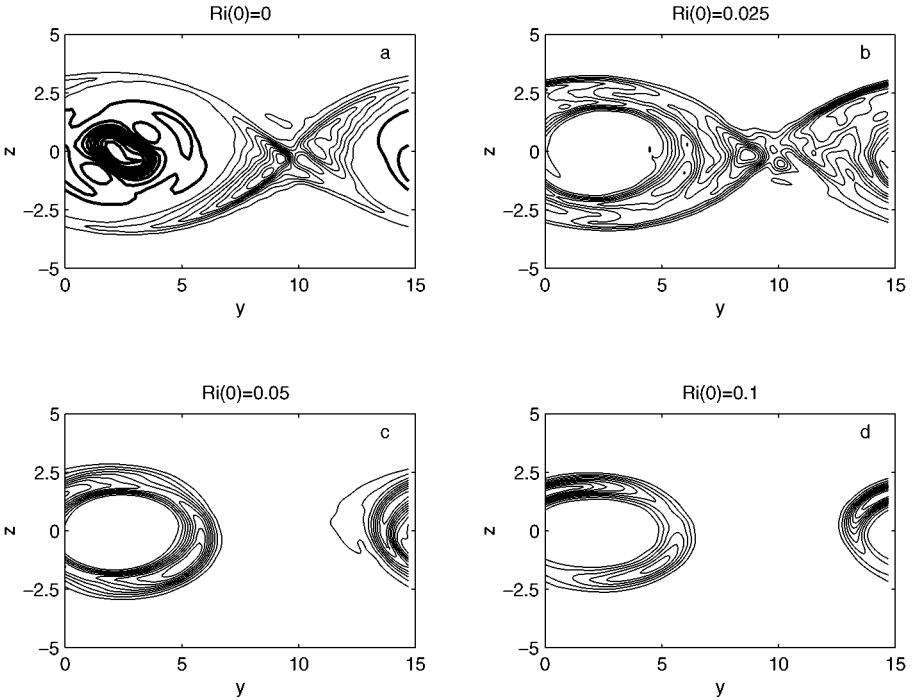

Figure 5 Contours of $\mathcal{K}_{3D}$ (as defined in Equation 16) for the most unstable three-dimensional mode in flows with Ri(0) = (*a*) 0 (*thin solid lines* show the most unstable (hyperbolic) mode with $\gamma = 2.5$, and *thick solid lines* show the most unstable elliptical mode with $\gamma = 0.9$); (*b*) 0.025; (*c*) 0.05; and (*d*) 0.1. [Adapted from figure 7 in Caulfield & Peltier (2000), used with permission.]

by these simulations, where the primary billows were so strongly disrupted by these secondary instabilities that transition occurred before subharmonic merging could take place.

The time-dependent evolution of cross-stream power spectra of the flow may be usefully invoked to test the quality of the further linear theoretic prediction of the expected cross-stream wavenumber γ of the three-dimensional secondary instability that is responsible, ultimately, for inducing complete turbulent collapse of the shear layer. Because the boundary conditions in the x-direction employed for the purpose of the DNS analyses are periodic, we may represent the streamwise component of the vorticity in the form of a Fourier series as

$$\omega_x(x, y, z, t) = \sum_{n=-N}^{+N} C_n(\gamma_n, y, z, t) e^{i\gamma nx}, \tag{17a}$$

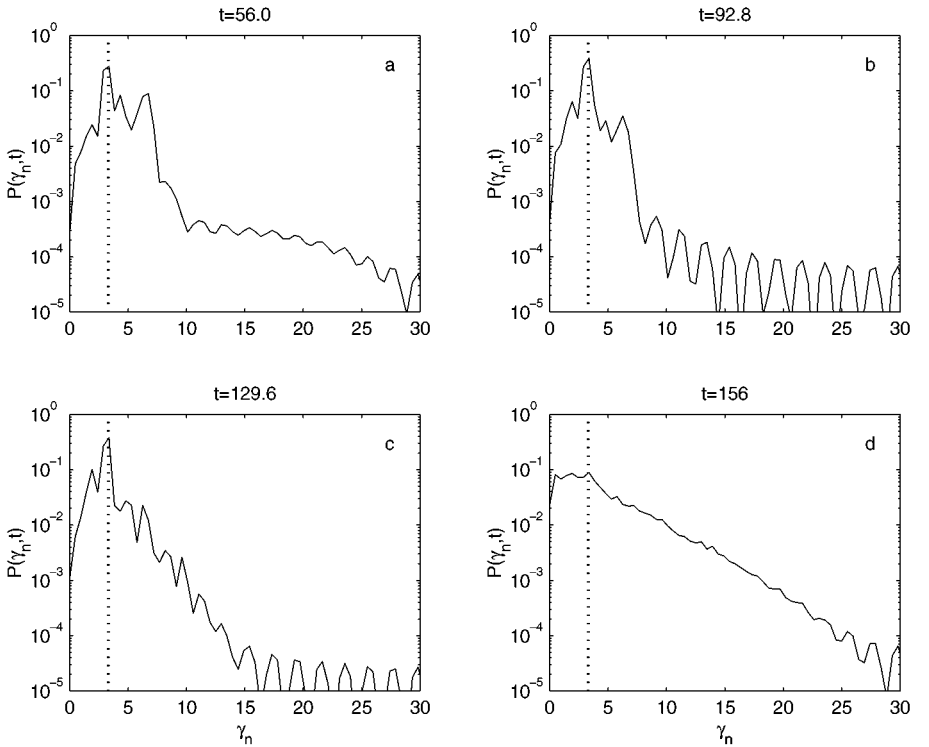

Figure 7 Variation of the various components of the normalized power spectrum density $P(\gamma_n, t)$ (defined in Equation 18) against γ_n at four characteristic times within a flow with $Ri(0) = 0.05$. The wavenumber of the most unstable spanwise mode shown in Figure 4 is denoted by a thick vertical dashed line.

with

$$C_n(\gamma_n, y, z, t) = \int_0^{L_x} \omega_x e^{-i\gamma n x}\, dx \tag{17b}$$

and $\gamma_n = n(2\pi/L_x)$, where L_x is the cross-stream width of the domain. Figure 7 shows the domain integral of the normalized spanwise power spectrum

$$P(\gamma_n, t) = \langle\langle |c(\gamma_n, y, z, t)|^2 \rangle_y \rangle_z. \tag{18}$$

Inspection of the results in Figure 7, on which the prediction of Floquet theory of the cross-stream wavenumber of the fastest growing mode of linear theory is shown as the vertical dashed line, demonstrates that this prediction of linear theory is precisely recovered by the detailed DNS analysis, thus verifying the assumption of a separation of timescales on the basis of which the stability analysis of the nonlinear KH waves was performed. By the time of the final frame of Figure 7

(t = 156 in nondimensional units), the power spectrum of the streamwise vorticity has assumed the "red" form that one expects of a strongly turbulent flow in which a cascade to small scales occurs following "injection" at the scale of the cross-stream mode of secondary instability. It is critical to appreciate that this scale is substantially smaller than the primary billow scale (by approximately one order of magnitude), and this has important implications for the mixing within the flow (discussed below). Indeed, it is clearly apparent that transition has occurred, as is expected because the flow Reynolds number is sufficiently high (see Dimotakis 2000). This is strong evidence to suggest that the crucial physical structures that trigger turbulence are not the primary billows, but rather the secondary convective instabilities that develop into streamwise vortices. The primary billows should be thought of as acting as catalysts, creating a flow that is conducive to the development of convective instabilities that develop to finite amplitude and then trigger transition. Important questions to address concern the mechanism or mechanisms by which the inherently three-dimensional streamwise vortices trigger transition as well as the mixing characteristics associated with the flow evolution, in particular, subsequent to this transition.

3.3. The Dominant Stage of Intense Three-Dimensional Mixing of the Stratified Parallel Flow

Kinetic energy diagnostics are shown in Figure 8 for four representative three-dimensional DNS. Figures 8*a*,*b*, and *c*, respectively, present the evolution of total kinetic energy of the flow $\mathcal{K}$, the cross-stream average perturbation kinetic energy of the flow $\mathcal{K}_{\rm KH}$, defined such that

$$\langle \mathcal{K} \rangle_x = \bar{\mathcal{K}} + \mathcal{K}_{\rm KH}, \tag{19a}$$

with

$$\bar{\mathcal{K}} = \langle (\bar{V}^2)/2 \rangle_z, \tag{19b}$$

and

$$\mathcal{K}_{\rm KH} = \left\langle \left\langle \left(v_{\rm KH}^2 + w_{\rm KH}^2 \right)/2 \right\rangle_y \right\rangle_z, \tag{19c}$$

and the three-dimensional deviation from this cross-stream average, which we are denoting by $\mathcal{K}_{\rm 3D}$ and which is defined as

$$\mathcal{K}_{\rm 3D} = \mathcal{K} - \bar{\mathcal{K}} - \mathcal{K}_{\rm KH}. \tag{19d}$$

This compartmentalization allows us to isolate the evolution of three dimensionality from the evolving two-dimensional KH billow component of the flow. Inspection of these diagnostics will demonstrate (from Figure 8*a*) that it is not until nondimensional time t > 100 that total kinetic energy begins to decrease rapidly owing to the intense viscous dissipation that onsets only with the proliferation of small spatial scales that develop during three-dimensional turbulent

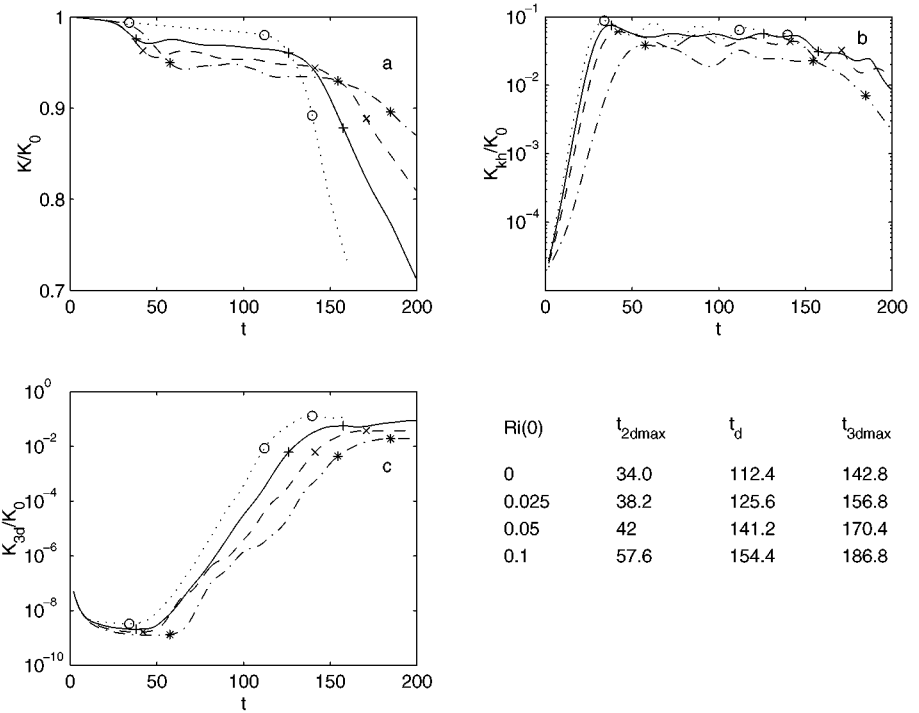

Figure 8 Time evolution of (*a*) $\mathcal{K}(t)/\mathcal{K}(0)$, (*b*) $\mathcal{K}_{KH}(t)/\mathcal{K}(0)$, and (*c*) $K_{3D}(t)/\mathcal{K}(0)$ for three-dimensional (as defined in Equations 3 and 19) simulations with Ri(0) = 0 (*dotted line*), Ri(0) = 0.025 (*solid line*), Ri(0) = 0.05 (*dashed line*), and Ri(0) = 0.1 (*dot-dashed line*). The characteristic times given in the table are marked with a circle [Ri(0) = 0], a plus [Ri(0) = 0.025], a cross [Ri(0) = 0.05], or an asterisk [Ri(0) = 0.1]. [Adapted from figure 8 in Caulfield & Peltier (2000), used with permission.]

transition and shear-layer collapse. Furthermore, the onset of three-dimensional perturbation growth is exactly coincident with the saturation of the primary KH billow, reinforcing the important conceptual idea that the two-dimensional billow serves merely to catalyze the development of three-dimensional motions. On each of these kinetic energy diagnostic time series, we have denoted by appropriate symbols three significant times in the evolution of the flow, respectively: the time t_{2Dmax} at which the two-dimensional KH instability achieves maximum amplitude; the time t_d at which the dissipation starts to grow markedly, signaling the onset of transition; and the time t_{3Dmax} at which the three-dimensional perturbations achieve maximum amplitude.

Figure 9 (*a–g*) illustrates the evolution of each of the reservoirs of potential energy ($\mathcal{P}$, $\mathcal{P}_A$, and $\mathcal{P}_B$) that accompanies the previously discussed evolution of the various components of kinetic energy. Results are shown for each of the seven

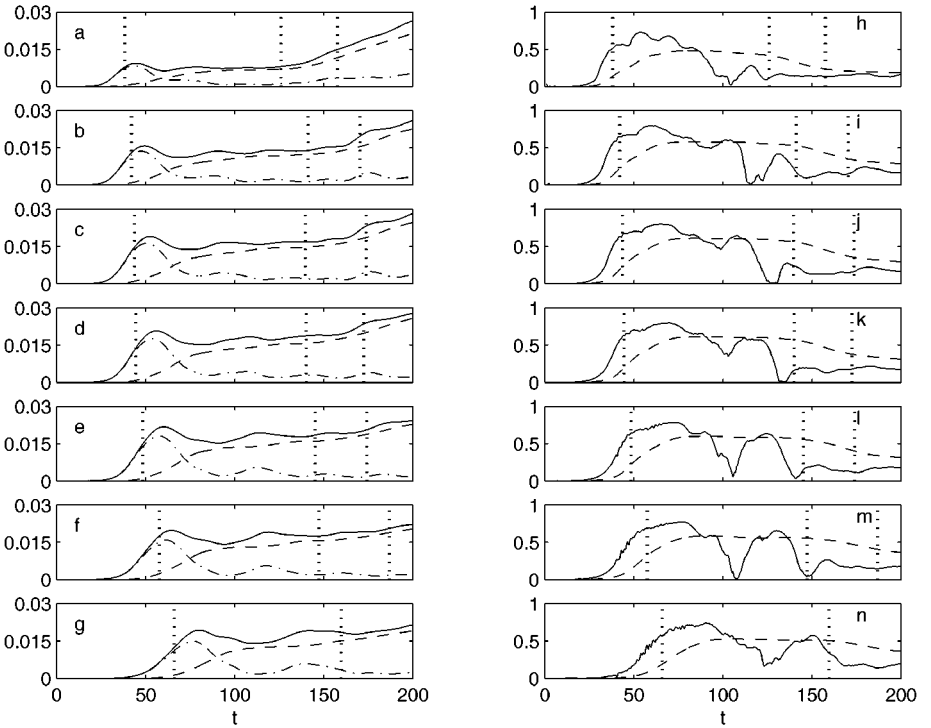

Figure 9 Time variation of $\mathcal{P}$(t)-$\mathcal{D}_{\rm Pt}$-$\mathcal{P}$(0) (*solid line*) (as defined in Equation 4), $\mathcal{P}_{\rm B}$(t)-$\mathcal{D}_{\rm Pt}$-$\mathcal{P}_{\rm B}$(0) (*dashed line*) (as defined in Equation 5), and $\mathcal{P}_{\rm A}$(t) (*dotted line*) (as defined in Equation 6) for inherently three-dimensional simulations with Ri(0) = (*a*) 0.025, (*b*) 0.05, (*c*) 0.0625, (*d*) 0.075, (*e*) 0.0875, (*f*) 0.1, and (*g*) 0.125, compared with the time variation of $\mathcal{E}_{\rm i}$ (*solid line*) and $\mathcal{E}_{\rm c}$ (*dashed line*) (as defined in Equations 8a–b) for inherently three-dimensional simulations with Ri(0) = (*h*) 0.025, (*i*) 0.05, (*j*) 0.0625, (*k*) 0.075, (*l*) 0.0875, (*m*) 0.1, and (*n*) 0.125. The characteristic times shown in Figure 5 are marked with thick vertical dotted lines.

stratified flows. The three key times discussed above in connection with the kinetic energy diagnostics are shown on each frame as the vertical dotted lines.

Directly after the saturation of the primary billows, for each simulation there is a phase of early time, "preturbulent" [using the nomenclature by Smyth et al. (2001)] mixing that is extremely efficient. The instantaneous efficiencies, which maximize subsequent to the time the two-dimensional waves saturate, reveal the influence of the nutation and oscillation of the billow core that follows saturation. Instantaneous mixing efficiency is observed to equal or exceed the high value of 0.75 near the time that the KH wave achieves maximum amplitude even though the flows remain highly coherent. It is apparent that $\mathcal{P}_{\rm B}$ only starts to increase once $\mathcal{P}_{\rm A}$ is large, and indeed much of the increase in $\mathcal{P}_{\rm B}$ occurs when the total

potential energy is decreasing (and so $\mathcal{H} > 0$ as defined in Equation 3). Thus the naïve definition of the flux Richardson number given by Equation 9a is not useful.

At these Reynolds numbers, this early-stage mixing is associated with the convectively unstable regions around the periphery of the primary vortex core, which naturally have the required characteristics for enhanced mixing (as discussed in Section 2), i.e., regions of static instability associated with a source of $\mathcal{P}_A$, and locally intensified density gradients. At sufficiently high Reynolds number, this region of the flow experiences enhanced small-scale mixing, as the available potential energy is imperfectly converted back into kinetic energy. This mixing is primarily due to the convective overturning that triggers the growth of the three-dimensional perturbations, in the regions around the periphery of the primary billow core (see Caulfield & Peltier 2000, where this identification could be made by the analysis of spatially compartmentalized three-dimensional perturbation growth), and nucleates the characteristic streamwise vortices, which, at sufficiently high Reynolds number, qualitatively change the long-time behavior of the flow.

Indeed, particularly for flows with weaker initial stratification, the total potential energy increases significantly at the same time as the total kinetic energy begins to decrease significantly (compare with Figure 8). It is important to note that this increase in potential energy at late time is not primarily due to a reversible exchange between the kinetic energy and the available potential energy reservoirs. Rather, the available potential energy $\mathcal{P}_A$ exhibits strong variability (necessary to enable irreversible mixing to occur) but of relatively small amplitude. The observed strong monotonic increase of total potential energy, at times later than the second characteristic time at which the dissipation starts to increase markedly, is clearly due to rapid increase in the background potential energy $\mathcal{P}_B$ of the flow, a further indication that it is in this latter stage of flow development in which significant three-dimensional irreversible mixing is occurring. In fact, enhanced three-dimensional irreversible mixing continues unabated during the entire post-transitional stage of flow development.

An important question to address clearly concerns the reason why this turbulence transition occurs. Once the convective instability develops, a large body of numerical evidence (see Palmer et al. 1996; Cortesi et al. 1998; Werne & Fritts 1999; Caulfield & Peltier 2000; Smyth & Moum 2000a,b; Smyth et al. 2001) points toward the inevitable development of disordered turbulent flow, with the streamwise vortices being driven to finite amplitude principally through vortex stretching by the mean shear, with the primary billows once again playing a primarily catalytic role.

It is apparent that the transition to turbulence is triggered by the catastrophic breakdown of these streamwise vortices. Owing to their location, the advection and amplification through stretching of the streamwise vortices by the background shear leads inevitably to the streamwise vortices propagating toward the braid region, and there comes an instant when these vortices collide. Such a finite amplitude subcritical interaction occurred in all the simulations analyzed here and appears to be the inevitable precursor to the onset of truly turbulent motions,

reinforcing the concept that it is the characteristic scale of the streamwise vortices, and not the significantly larger primary billow scale, that is the dominant injection scale for the turbulent cascade. Indeed, owing to the unsteadiness of the flow, it appears not to be appropriate to consider the development of tertiary instabilities of the streamwise vortices to be the trigger for transition. Rather, subcritical, finite amplitude vortex-vortex interactions seem to be the primary cause. Indeed, the numerical evidence appears to point to the requirement not only of adequate resolution of individual streamwise vortices, but also of sufficient spanwise expanse so that multiple streamwise vortices can develop and interact during transition in order to capture properly the transition behavior.

However, it is important to stress that there is some evidence (Arendt et al. 1997, Fritts et al. 1998) that the streamwise vortices may support a family of propagating disturbances, referred to as Kelvin twist waves (see Arendt et al. 1997, Fritts et al. 1998 for a full discussion). These disturbances, which propagate along the vortex tubes [and appear to arise naturally as a part of any initial disturbance on the vortex (as demonstrated by Arendt et al. 1997)], can lead to fragmentation and depletion of the vortex tubes, thus triggering transition to smaller and smaller scales of motion within the flow. Arendt et al. (1997) and Fritts et al. (1998) also found that vortex-vortex interactions with longer wavelengths [associated with the cooperative Crow (1970) instability of neighboring elliptical vortices] could also induce turbulence, and it is not yet clear which of these competing mechanisms, if either, plays an active role in the transition process.

However, it is clear that the turbulence transition is intimately related to the streamwise vortices induced by convective instability, as first described by Klaassen & Peltier (1985b), and that they are the primary mechanism by which enhanced dissipation is triggered within stratified shear flows. The issue as to whether this turbulence transition mechanism is the dominant mechanism in all stratified shear flows is highly complex, with the relative importance of the various stages of flow evolution depending on both the flow parameters and the strength of the initial forcing. For example, if the flow is forced so that merging events can occur before the transition to turbulence, the mixing associated with the coherent, and essentially two-dimensional, merging of neighboring vortices can constitute a dominant part of the total mixing experienced within the flow, as discussed by Smyth et al. (2001).

Also, and as is apparent for the more strongly stratified simulation [with $\mathrm{Ri}(0) = 0.125$], the mixing associated with the preturbulent overturning in the convective layers is very intense and constitutes a significant proportion of the total mixing experienced by this flow. As is apparent in Figure 8*b*, the growth of the primary KH billow in this flow is relatively weak, owing to the stabilizing effect of stratification on this simulation. Also, as is apparent in Figure 8*c*, increasing stratification also reduces the growth rate of the developing three-dimensional perturbations, and their saturation amplitude also reduces as the stratification increases. Such weakening growth of the primary KH instability for $\mathrm{Ri}(0) > 0.1$ is commonly observed in laboratory experiments (see Koop & Browand 1979,

Linden 1979, Thorpe 1987, Fernando 1991). However, the crucial influence of sufficiently high stratification actually appears to be the reduction in the saturated amplitude of the three-dimensional perturbations, which, we believe, is indicative of a qualitative change in the character of the flow.

Such behavior is also observed in numerical simulations of flows with constant shear and density gradient, which are likely to have certain points of connection with the turbulent flows considered here because the characteristic scales of motion are becoming small compared to the mean shear and density gradient. As identified by several authors (Holt et al. 1992, Jacobitz et al. 1997, Diamessis & Nomura 2002), the growth of turbulent kinetic energy is inhibited by buoyancy forces for $\mathrm{Ri} > 0.1$ in such flows. Our results are strongly suggestive of an analogous behavior, with a relatively short period of turbulent disordered motion occurring for the flows with higher Ri(0), whereas the less strongly stratified simulations exhibit extended periods of turbulent mixing, leading to much greater total mixing than occurs in the initial preturbulent phase. The relative importance of these two phases is likely to also depend on the Reynolds number of the flow, as lower Reynolds number will tend to reduce the significance of the turbulent phase at a given stratification from the high *Re* behavior that shows a demarcation around $\mathrm{Ri}(0) = 0.1$.

Nevertheless, in all the simulations we discuss here, it is clear that after transition occurs the absolute value of the background potential energy begins to grow. This is particularly noticeable for flows with smaller initial stratification, where the preturbulent convective overturning has achieved little mixing, yet the streamwise vortices that are induced by this overturning grow rapidly and then trigger significantly increased mixing and strong dissipation. This behavior, as is apparent from the spectra shown in Figure 7, occurs at substantially smaller scale than both the primary KH instability and the injection scale of the secondary convective rolls, thereby further reinforcing the analogy with the constant shear/constant density gradient simulations.

Based on the use of Equations 8a and 8b, we show in Figure 9*h–n* the evolution of the mixing efficiency, both instantaneous (*solid lines*) and cumulative (*dashed lines*), for each of the seven stratified flow examples for which we have performed detailed analysis. In this range of time during which three-dimensional motions have proliferated and intense viscous dissipation is occurring, a state that is "turbulent" in the conventional sense, the instantaneous mixing efficiency has decreased substantially toward the experimentally determined value of approximately 0.2–0.3 that is characteristic of mixing associated with shear instabilities (e.g., Linden 1979, Figure 4, where the flux Richardson number has been averaged over a sufficiently long timescale for equality to be obtained between $\mathrm{R_f}$ and $\mathcal{E}_c$).

Particularly for flows with lower characteristic stratification, this phase of flow evolution dominates the overall mixing character of the ultimate flow. In the next section, we discuss this late stage in more detail, drawing connections between the properties of this late stage with experimental and theoretical investigations of mixing within stratified flows, paying particular attention to the implications of the variation of mixing efficiency with stratification during this turbulent phase.

4. TURBULENT-MIXING EFFICIENCY AS A FUNCTION OF RICHARDSON NUMBER

Because the late, turbulent stage of flow evolution appears to be so important, it is therefore useful to redefine the cumulative mixing efficiency as a function of time t subsequent to the onset of true three-dimensional turbulent mixing. This quantity, denoted E_c^t, is shown in Figure 10*a* for several flows that differ from one another in terms of their initial Richardson number. Inspection of these results shows that there exists clear evidence of nonmonotonicity of the mixing efficiency as a function of the initial Richardson number. Also shown in Figure 10*b–d* are the mean fields of density, horizontal velocity, and ρ_B at the time $t - t_{3Dmax} = 40$ for the three-dimensional flows with $Ri(0) = 0.025$, 0.05, and 0.1, respectively, showing clear evidence of the development of an intermediate layer of well-mixed fluid when $Ri(0) = 0.05$.

Averaging over the interval for which results are shown in Figure 10*a* for the cumulative mixing efficiency, we obtain the efficiency versus initial Richardson numbered diagram shown in Figure 11*a*. Here we have plotted the results obtained for seven nonzero values of the initial Richardson number. Inspection of the results plotted on Figure 11*a* clearly shows that the efficiency with which the density field is mixed in the turbulent regime is a strongly nonmonotonic function of the stratification and moreover that the range of efficiencies that we have inferred is in accord with the values that have been obtained from laboratory measurements.

As originally conjectured by Phillips (1972) and Posmentier (1977), nonmonotonicity in the mixing efficiency should lead to the development of distinct layers within the stratified fluid. Physically, this can be understood (see Linden 1979 for a clear discussion) by considering a location where the density gradient is locally increased relative to neighboring values. If the mixing efficiency is a decreasing function of stratification in this vicinity, the flux of buoyancy above and below this particular level will be greater, where the stratification is weaker, thus leading to accumulation at this location and hence intensification of the local gradient.

Such nonmonotonicity and dependence of the mixing efficiency purely on the overall stratification requires that the dominant scales of mixing should be small compared to the density gradient. Although this is not true of the early stages of shear-flow development (where the characteristic scale of the flow is that of the primary billow), the evidence from the numerical simulations points to the scales of mixing at later times being substantially smaller than the injection scale of the streamwise vortices characteristic of the secondary convective instability, thus indeed being smaller than the stratification scales.

It is unfortunate that the simple physical model presented by Linden (1979) leads to a mathematically ill-posed problem, as pointed out by Barenblatt et al. (1993). They showed, however, that if a finite time lag existed for the turbulence to adjust to the ambient stratification, then the problem became well posed, leading to the development of finite layers. Consideration of the late-time behavior of a stratified shear layer points to just such a finite time lag, as can be inferred

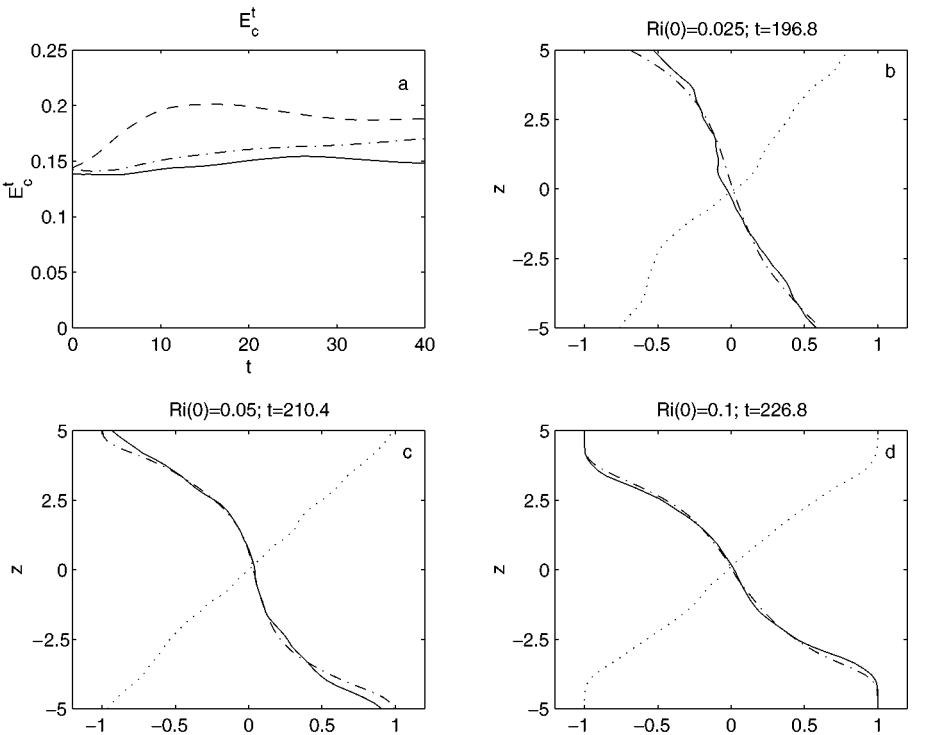

Figure 10 (*a*) Variation of the posttransition cumulative mixing efficiency ($\mathcal{E}_c^t$) with t-t_{3dmax} (listed in Figure 8) for inherently three-dimensional simulations with Ri(0) = 0.025 (*solid line*), 0.05 (*dashed line*), and 0.1 (*dot-dashed line*). Vertical profiles of horizontally averaged velocity (*dotted line*), horizontally averaged density (*solid line*), and background density ρ_B (*dot-dashed line*) at the time t-t_{3dmax} = 40 (listed in Figure 8) for three-dimensional flows with Ri(0) = (*b*) 0.025, (*c*) 0.05, and (*d*) 0.1. [Adapted from figure 10 of Caulfield & Peltier (2000), used with permission.]

from the mixing data shown in Figure 9. As already mentioned, nonzero available potential energy is a necessary condition for irreversible mixing processes to occur within the fluid, and such intermediate creation of $\mathcal{P}_A$ occurs on the timescale of the turnover of the turbulent eddies within the flow, yielding a mechanism consistent with that postulated by Barenblatt et al. As is clearly demonstrated in Figure 10, an intermediate well-mixed layer does indeed develop for intermediate stratifications.

A further important point that needs to be noted is that there is a qualitative change in the behavior of the flow for larger values of Ri(0), with the efficiency increasing again at higher stratifications. This appears to be due to the fact that the dissipation ε is decreasing owing to the reduced intensity of the streamwise vortices at late times, whereas the quantity of mixing associated with this breakdown does

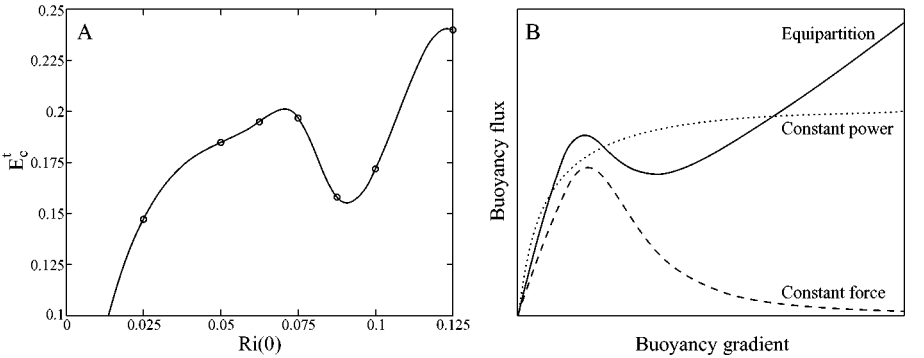

Figure 11 (*a*) Variation of the time-averaged value of the posttransition cumulative mixing efficiency ($\mathcal{E}_c^t$) with Richardson number for the seven simulations shown in Figure 9 (the connecting curve is generated by cubic spline interpolation). (*b*) Schematic illustration of three possible relations between the buoyancy gradient and buoyancy flux for turbulent-mixing experiments as proposed by Balmforth et al. (1998). The three curves correspond to the assumption that forcing exerts constant force per unit mass (*dashed line*), with constant power (*dotted line*) or "equipartition" (*solid line*) implying turbulent eddies adjust to an external velocity scale on the eddy turnover timescale. [Figure 11*b* is adapted from figure 1 in Balmforth et al. (1998), used with permission.]

not decrease, owing at least in part to the increased stratification and, hence, to the increased characteristic density differences in the flow.

This behavior is somewhat suggestive of the variation of buoyancy flux with overall stratification that was recently conjectured by Balmforth et al. (1998) in an attempt to develop a model to explain the layer formation observed in experiments attributed to Park et al. (1994). Balmforth et al. (1998) postulated, using mixing-length theory, that such a variation in buoyancy flux (as shown in Figure 11*b*) could occur if the characteristic eddy speed for turbulent motions within a stratified fluid adjusted to an external driving velocity (in this case, that of the stirring rods) on the timescale of an eddy turnover. Within the framework of a stratified shear flow, the analogous assumption is that the streamwise vortices, associated with the convective instability, are intensified (and hence driven to mixing) by the background shear on a timescale comparable with their turnover time, essentially that which occurs during the relatively rapid period of turbulence onset within the flow. This gives further support to the observation that stratified mixing driven by the breakdown of secondary streamwise vortices may lead to the creation of a "staircase" density structure.

5. CONCLUSIONS

In this paper, we review and somewhat extend our own recent work on the inference of mixing efficiency in stratified parallel flows that undergo the process of turbulent collapse. This process begins with the onset of a two-dimensional, essentially

inviscid, KH instability. As the two-dimensional KH billows saturate, the rate of change with time of the two-dimensional fields is sufficiently slow to allow for the emergence of a secondary instability. This secondary instability is convective in nature and is initially focused in the regions of overturning isopycnals that are induced by the rolling-up of the vorticity into the cat's-eye structures that characterize the individual billows. It also consists of streamwise vortex streaks of alternating sign in the transverse direction. As these streamwise vortices amplify, they are stretched in the streamwise direction and eventually interact with those associated with the adjacent billow core. This final stage of interaction results in the dramatic loss of spatial coherence and the sharp rise of viscous dissipation that characterizes the "mixing transition," and particularly for smaller values of the flow stratification, this late stage of evolution dominates the mixing within the flow.

As demonstrated through discussion of the detailed theoretical analyses in Section 3, the efficiency of the mixing process varies considerably during the three primary stages of transition. Immediately after the initial stage of two-dimensional KH instability amplification, the efficiency of mixing according to our definition is extremely high, although the amount of mixing can be small, owing to the fact that this stage is fundamentally laminar. This mixing is associated with the nucleation of the secondary instabilities, which play the essential role in the mixing transition. During the final stage of three-dimensional turbulent collapse, on the contrary, the mixing efficiency is small and on the order of 0.2, in accord with the experimental measurements. In this stage, however, the amount of mixing can be high, provided the stratification is sufficiently weak for intense development of the secondary instabilities. The stage of flow evolution through which these two asymptotic regimes of behavior are connected, that which is associated with the three-dimensional coherent structures that are referred to in the experimental literature as vortex streaks, is clearly critical to the transition process. It is during this short-lived regime that viscous dissipation first begins to rise significantly because the spatial scale of these streaks is an order of magnitude less than the spatial scale of the parent KH billow.

It is important to note that the efficiency with which the density field is mixed during the "mixing transition" in stably stratified parallel flow is a nonmonotonic function of the initial minimum gradient Richardson number of the flow. Both Philips (1972) and Posmentier (1977) have proposed on theoretical grounds that such nonmonotonicity should be a generic property of the mixing induced by small-scale turbulence. Barenblatt et al. (1993) have specifically argued that such dependence inevitably leads to the formation of a vertical "staircase" variation of density, provided there is an adjustment time of the turbulence to the ambient stratification, which is also characteristic of the stratified shear-flow transition problem. However, theoretical, numerical, and experimental suggestions indicate (see Balmforth et al. 1998, Caulfield & Kerswell 2001, Strang & Fernando 2001) (also see Figure 11) that there is a further regime to be explored at higher ambient stratifications and that more complicated background flows may lead to higher efficiencies of, still turbulent, mixing.

Indeed, strong experimental evidence for the occurrence of a change in the behavior of the mixing as the primary KH billows reduce in importance has been presented recently by Strang & Fernando (2001). When their flow was visually susceptible to primary KH instabilities, they found measured values of appropriately averaged flux Richardson numbers (which could be identified with $\mathcal{E}_c^t$, as shown in Figures 10 and 11) of the order of 0.2–0.3. However, with their particular experimental design, increasing total stratification inevitably led to a reduction in the relative depth of the region of density variation, and so for larger values of ambient stratification, Holmboe waves also developed. The interaction between the two coexisting instabilities led to substantially higher mixing efficiencies, on the order of 0.4–0.5 for intermediate stratifications. As the stratification was further increased, the mixing efficiency then dropped substantially, providing evidence that such strongly stratified flows were not greatly susceptible to flow instabilities of any kind. Nevertheless, the accumulating evidence suggests that layering in the stratification and efficiencies of the order of 0.2 are characteristic of mixing catalyzed by the development of KH instabilities and are driven by the associated secondary convective instabilities.

In this review, we illustrate the crucial variations of mixing efficiency with stratification that occur with relatively simple initial profiles of velocity and density. It will be necessary to consider the mixing associated with a much wider range of initial flow conditions before really useful parameterizations of this complex problem can be developed, with three main avenues of attack being apparent. First, the effect of variation with Prandtl number, as initially explored by Klaassen & Peltier (1985a) and Smyth et al. (2001), will have to be investigated in detail at sufficiently high Reynolds number and Peclet number to have an intense turbulent-mixing phase, as the existence of such a phase has been shown to be crucial to the mixing within the flow.

Second, a wider range of flow profiles must be considered because, as shown experimentally by Strang & Fernando (2001), interactions between instabilities of various kinds seem to lead to qualitatively different mixing properties. An interesting, still unanswered, question to be addressed is whether the mixing efficiency associated with secondary instabilities catalyzed by primary KH instabilities is a generic property of stratified shear flows, or is it special to the particular initial conditions subject to primary KH instabilities. Although parameterizations, such as those by Mellor & Yamada (1982), do essentially make this assumption, by restricting R_f to be at most 0.3 or so, recent experimental (Strang & Fernando 2001) and observational (Pardyjak et al. 2002) evidence suggests the possibility of mixing efficiencies of the order of 0.4–0.5 in certain circumstances. In other words, the evidence points toward the possibility that the kinetic energy of the flow may be lost equally to viscous dissipation and irreversible mixing. Such behavior may be characteristic of a stratified Couette flow, if the flow is able to attain the theoretical maximum upper bound for mixing (see Caulfield & Kerswell 2001), and was postulated on scaling grounds by Townsend (1958) for statistically steady turbulent flow. It would be of great practical interest to be able to identify such

behavior in a time-dependent simulation of a stratified turbulent flow, analyzed using the formalism reviewed in Section 2.

Finally, and perhaps most importantly, the interaction of turbulent mixing with the internal gravity wave spectrum must be considered (e.g., as in Sutherland & Peltier 1994). Internal waves lead inevitably to both temporal and spatial variability in the underlying flow, and so the effect of time variation in the background flow on the development of shear instabilities should be investigated. Also, internal waves provide a mechanism by which energy and momentum can be transported away from their generation region (Sutherland & Peltier 1995), and thus the inclusion of gravity wave dynamics within the flow may have a qualitatively important effect on the energy and momentum budgets. Understanding the interplay between the wave-like and eddy-like parts of realistic flows is clearly the major remaining challenge for developing an understanding of stratified mixing and for realizing the full geophysical relevance of studies such as those reviewed and extended here.

LITERATURE CITED

Arendt S, Fritts DC, Andreassen O. 1997. The initial value problem for Kelvin vortex waves. *J. Fluid Mech.* 344:181–212

Balmforth NJ, Llewellyn Smith SG, Young WR. 1998. Dynamics of interfaces and layers in a stratified turbulent fluid. *J. Fluid Mech.* 355:329–58

Barenblatt GI, Bertsch M, Dal Paso R, Prostokishin VM, Ughi M. 1993. A mathematical model of turbulent heat and mass transfer in stably stratified shear flow. *J. Fluid Mech.* 253:341–58

Browand FK, Winant CD. 1973. Laboratory observations of shear instability in a stratified fluid. *Bound.-Layer Meteorol.* 5:67–77

Caulfield CP, Kerswell RR. 2001. Maximal mixing rate in turbulent stably stratified Couette flow. *Phys. Fluids* 13:894–900

Caulfield CP, Peltier WR. 1994. Three-dimensionalization of the stratified mixing layer. *Phys. Fluids* 6:3803–5

Caulfield CP, Peltier WR. 2000. The anatomy of the mixing transition in homogeneous and stratified free shear layers. *J. Fluid Mech.* 413:1–47

Cortesi AB, Yadigaroglu G, Bannerjee S. 1998. Numerical investigation of the formation of three-dimensional structures in stably stratified mixing layers. *Phys. Fluids* 10:1449–73

Crow SC. 1970. Stability theory for a pair of trailing vortices. *AIAA J.* 8:2172

Davis PA, Peltier WR. 1979. Some characteristics of the Kelvin-Helmholtz and resonant over-reflection modes of shear flow instability and of their interaction through vortex pairing. *J. Atmos. Sci.* 36:2394–412

De Silva IPD, Fernando HJS, Eaton F, Hebert D. 1996. Evolution of Kelvin-Helmholtz billows in nature and laboratory. *Earth Planet. Sci. Lett.* 143:217–31

Diamessis PJ, Nomura KK. 2002. The structure and dynamics of overturns in stably stratified homogeneous turbulence. *J. Fluid Mech.* Submitted

Dimotakis PE. 2000. The mixing transition in turbulent flows. *J. Fluid Mech.* 409:69–98

Drazin PG, Reid WH. 1981. *Hydrodynamic Stability*. Cambridge, MA: Cambridge Univ. Press

Fernando HJS. 1991. Turbulent mixing in stratified fluids. *Annu. Rev. Fluid Mech.* 23:455–93

Fritts DC, Arendt S, Andreassen O. 1998. Vorticity dynamics in a breaking internal gravity

wave. Part 2. Vortex interactions and transition to turbulence. *J. Fluid Mech.* 367:47–65

Gerz T, Schumann U, Elghobashi SE. 1989. Direct numerical simulation of stratified homogeneous turbulent shear flows. *J. Fluid Mech.* 200:563–94

Holmboe J. 1962. On the behaviour of symmetric waves in stratified shear layers. *Geofys. Publ. Oslo* 24:67–113

Holt SE, Koseff JR, Ferziger JH. 1992. A numerical study of the evolution and structure of homogeneous stably stratified sheared turbulence. *J. Fluid Mech.* 237:499–539

Howard LN. 1961. Note on a paper of John W. Miles. *J. Fluid Mech.* 10:509–12

Jacobitz FG, Sarkar S, Van Atta CW. 1997. Direct numerical simulations of the turbulence evolution in a uniformly sheared and stably stratified flow. *J. Fluid Mech.* 342:231–61

Keller KH, Van Atta CW. 2000. An experimental investigation of the vertical temperature structure of homogeneous stratified shear turbulence. *J. Fluid Mech.* 425:1–29

Kerswell RR. 2002. Elliptical instability. *Annu. Rev. Fluid Mech.* 34:83–113

Klaassen GP, Peltier WR. 1985a. Prandtl number effects on the evolution and stability of finite amplitude Kelvin-Helmholtz billows. *Geophys. Astrophys. Fluid Dyn.* 32:23–60

Klaassen GP, Peltier WR. 1985b. The onset of turbulence in finite amplitude Kelvin-Helmholtz billows. *J. Fluid Mech.* 155:1–35

Klaassen GP, Peltier WR. 1989. The role of transverse secondary instabilities in the evolution of free shear layers. *J. Fluid Mech.* 202:367–402

Klaassen GP, Peltier WR. 1991. The influence of stratification on secondary instabilities in free shear layers. *J. Fluid Mech.* 227:71–106

Koop G, Browand FK. 1979. Instability and turbulence in stratified fluids. *J. Fluid Mech.* 93:135–59

Lawrence GA, Browand FK, Redekopp LG. 1991. The stability of a sheared density interface. *Phys. Fluids A* 3:2360–70

Linden PF. 1979. Mixing in stratified fluids. *Geophys. Astrophys. Fluid Dyn.* 13:2–23

Lorenz EN. 1955. Available potential energy and the maintenance of the general circulation. *Tellus* 7:157–67

Mellor GL, Yamada T. 1982. Development of a turbulence closure model for geophysical fluid problems. *Rev. Geophys. Space Phys.* 20:851–75

Miles JW. 1961. On the stability of heterogeneous shear flows. *J. Fluid Mech.* 10:496–508

Palmer TL, Fritts DC, Andreassen O. 1996. Evolution and breakdown of Kelvin-Helmholtz billows in stratified compressible flows. 1. Instability structure, evolution and energetics. *J. Atmos. Sci.* 53:3192–212

Palmer TL, Fritts DC, Andreassen O, Lie I. 1994. Three-dimensional evolution of Kelvin-Helmholtz billows in stratified compressible flow. *Geophys. Res. Lett.* 21:2287–90

Pardyjak ER, Monti P, Fernando HJS. 2002. Flux Richardson number measurements in stable atmospheric shear flows. *J. Fluid Mech.* 459:307–16

Park YG, Whitehead JA, Gnanadeskian A. 1994. Turbulent mixing in stratified fluids, layer formation and energetics. *J. Fluid Mech.* 279:279–312

Peltier WR, Hallé J, Clark TL. 1978. The evolution of finite-amplitude Kelvin-Helmholtz billows. *Geophys. Astrophys. Fluid Dyn.* 10:53–87

Phillips OM. 1972. Turbulence in a strongly stratified fluid is unstable? *Deep Sea Res.* 19:79–81

Pierrehumbert RT, Widnall SE. 1982. The two- and three-dimensional instabilities of a spatially periodic shear layer. *J. Fluid Mech.* 114:59–82

Posmentier ES. 1977. The generation of salinity fine structures by vertical diffusion. *J. Phys. Oceanogr.* 7:298–300

Potylitsin P, Peltier WR. 1998. Stratification effects on the stability of columnar vortices on the f-plane. *J. Fluid Mech.* 355:45–79

Potylitsin P, Peltier WR. 1999. Three-dimensional destabilization of Stuart vortices: the influence of rotation and ellipticity. *J. Fluid Mech.* 387:205–26

Scinocca JF. 1995. The mixing of mass and momentum by Kelvin-Helmholtz billows. *J. Atmos. Sci.* 52:2509–30

Smyth WD, Klaassen GP, Peltier WR. 1988. Finite amplitude Holmboe waves. *Geophys. Astrophys. Fluid Dyn.* 43:181–222

Smyth WD, Moum JN. 2000a. Anisotropy of turbulence in stably stratified mixing layers. *Phys. Fluids* 12:1343–62

Smyth WD, Moum JN. 2000b. Length scales of turbulence in stably stratified mixing layers. *Phys. Fluids* 12:1327–42

Smyth WD, Moum JN, Caldwell DR. 2001. The efficiency of mixing in turbulent patches: inferences from direct simulations and microstructure observations. *J. Phys. Oceanogr.* 31:1969–92

Smyth WD, Peltier WR. 1994. Three-dimensionalization of barotropic vortices on the f-plane. *J. Fluid Mech.* 265:25–64

Smyth WD, Winters KB. 2002. Turbulence and mixing in Holmboe waves. *J. Phys. Oceanogr.* Submitted

Strang EJ, Fernando HJS. 2001. Entrainment and mixing in stratified shear flows. *J. Fluid Mech.* 428:349–86

Sutherland BR, Caulfield CP, Peltier WR. 1994. Internal wave generation and hydrodynamic instability. *J. Atmos. Sci.* 51:3261–80

Sutherland BR, Peltier WR. 1994. Turbulence transition and internal wave generation in density stratified jets. *Phys. Fluids A* 6:1267–84

Sutherland BR, Peltier WR. 1995. Internal wave emission into the middle atmosphere from a model tropospheric jet. *J. Atmos. Sci.* 52:3214–35

Thorpe SA. 1977. Turbulence and mixing in a Scottish loch. *Philos. Trans. R. Soc. London Ser. A* 286:125–81

Thorpe SA. 1987. Transitional phenomena and the development of turbulence in stratified fluids: a review. *J. Geophys. Res.* 92C:5231–48

Townsend AA. 1958. The effects of radiative transfer on turbulent flow of a stratified fluid. *J. Fluid Mech.* 4:361–75

Tseng Y-H. Ferziger JH. 2001. Mixing and available potential energy in stratified flows. *Phys. Fluids* 13:1281–93

Werne J, Fritts DC. 1999. Stratified shear turbulence: evolution and statistics. *Geophys. Res. Lett.* 26:439–42

Winters KB, D'Asaro EA. 1996. Diascalar flux and the rate of fluid mixing. *J. Fluid Mech.* 317:179–93

Winters KB, Lombard PN, Riley JJ, D'Asaro EA. 1995. Available potential energy and mixing in density-stratified fluids. *J. Fluid Mech.* 289:115–28

Woods JD. 1968. Wave-induced shear instability in the summer thermocline. *J. Fluid Mech.* 32:791–800

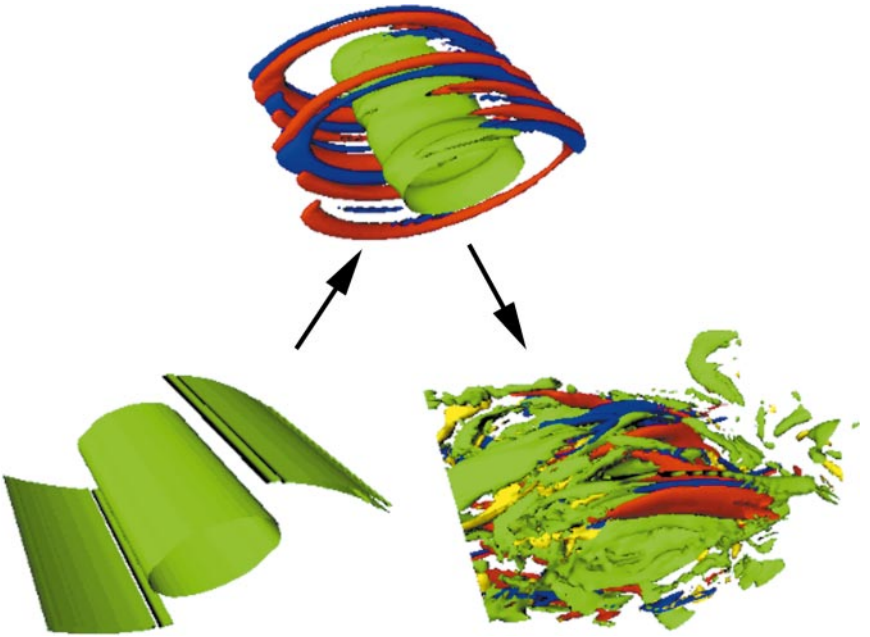

Figure 3 Isosurfaces of spanwise vorticity (green), streamwise vorticity of opposite signs (red and blue), and absolute value of vertical vorticity (yellow) for a simulation with Re $=$ 750, Pr $=$ 1, and Ri(0) $=$ 0.05 at three characteristic times (t_{2dmax}): when the two-dimensional perturbation has maximal amplitude, when the kinetic energy associated with the three-dimensional perturbation is 1% of the kinetic energy associated with the two-dimensional perturbation, and when the dissipation within the flow is maximal.

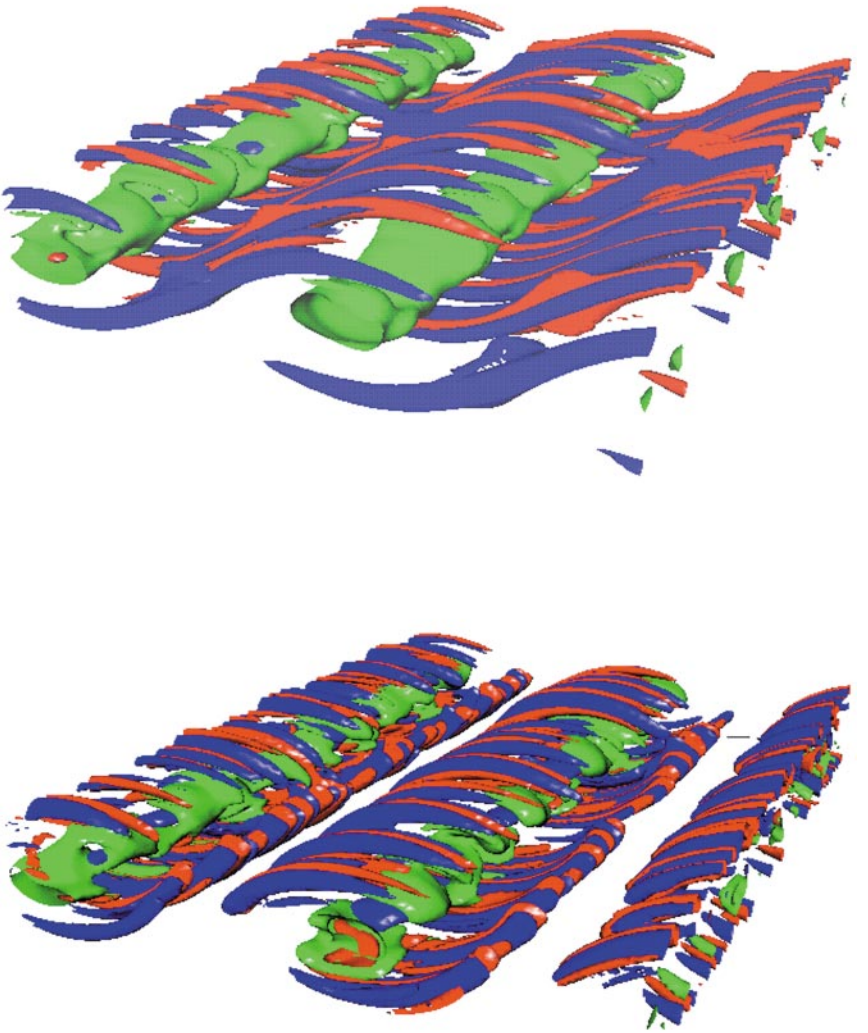

Figure 6 Isosurfaces of spanwise vorticity (green) and positive (blue) and negative (red) streamwise vorticity within (*a*) unstratified and (*b*) stratified (with $\mathrm{Ri}(0) = 0.05$) simulations containing two neighboring primary Kelvin-Helmholtz billows, during the development of intense spanwise-periodic streamwise vortices.

Annual Review of Fluid Mechanics
Volume 35, 2003

CONTENTS